

AD-A 236,641

NASA-CR-188,676

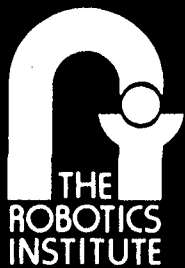
NASA-CR-188676  
19910018240

**Experimental Characterization of the**

**Perceptron Laser Rangefinder**

**In So Kweon, Regis Hoffman, and Eric Krotkov**

**CMU-RI-TR-91-1**



---

**Carnegie Mellon University**

---

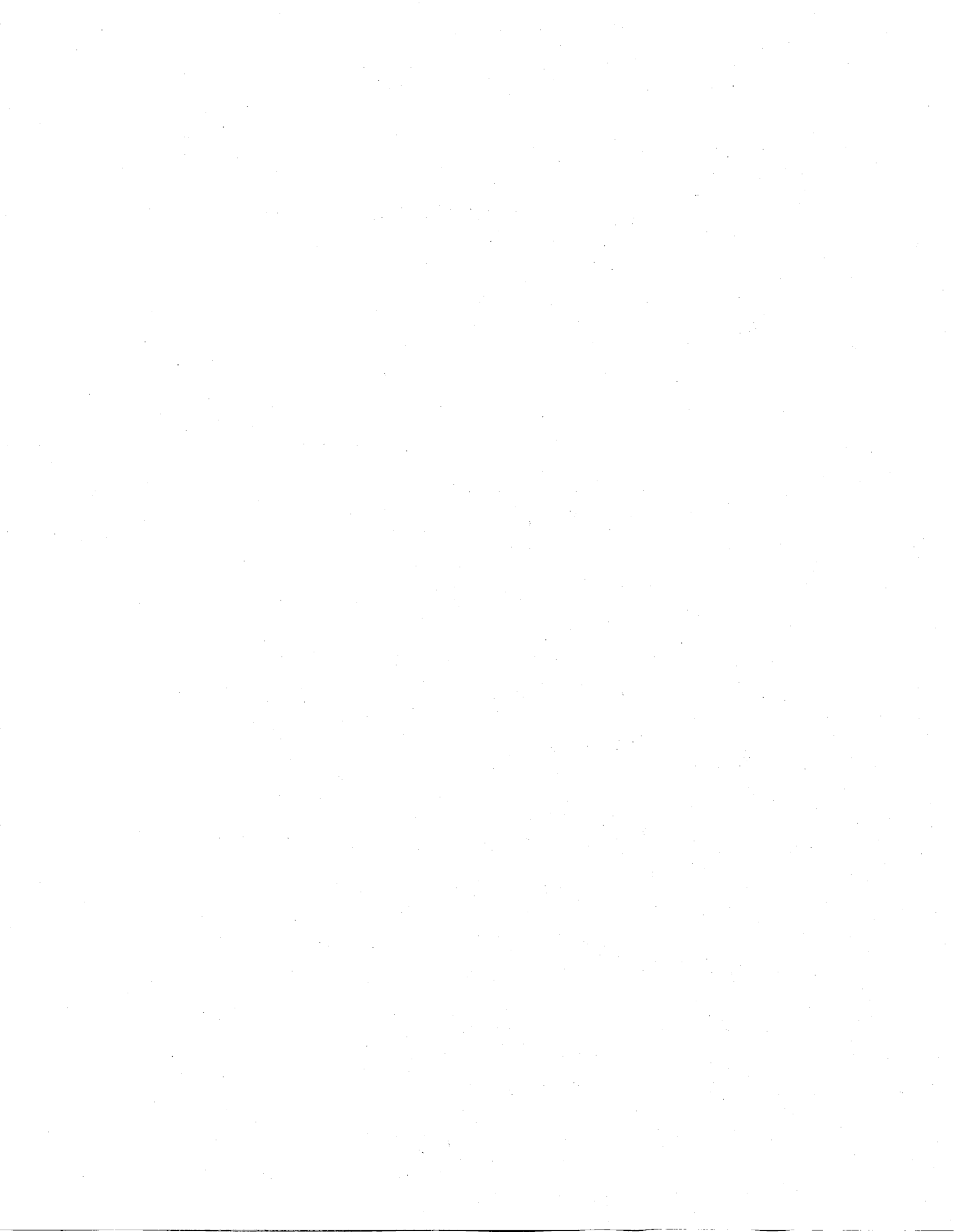
**The Robotics Institute**

---

**Technical Report**

---

---



ENTER:

4B

EM3287.PRT

DISPLAY 02/6/4

91N27554\*# ISSUE 19 PAGE 3175 CATEGORY 37 RPT#: NASA-CR-188676 NAS

1.26:188676 AD-A236641 CMU-RI-TR-91-01 CNT#: NAGW-1175 91/01/00 51

PAGES UNCLASSIFIED DOCUMENT

UTTL: Experimental characterization of the perceptron laser rangefinder

AUTH: A/KWEON, I. S.; B/HOFFMAN, REGIS; C/KROTKOV, ERIC

CORP: Carnegie-Mellon Univ., Pittsburgh, PA. CSS: (Robotics Inst.)

SAP: Avail: NTIS HC/MF A04

CIO: UNITED STATES

MAJS: /\*ACCEPTABILITY/\*ACCURACY/\*DETECTION/\*IMAGE RESOLUTION/\*LASER RANGE

FINDERS/\*OPTICAL SCANNERS/\*PERFORMANCE TESTS

MINS: / INDEPENDENT VARIABLES/ LIGHT (VISIBLE RADIATION)/ PRECISION/ REFLECTANCE

/ REFLECTION

ABA: GRA

Handwritten text, possibly bleed-through from the reverse side of the page. The text is extremely faint and illegible.



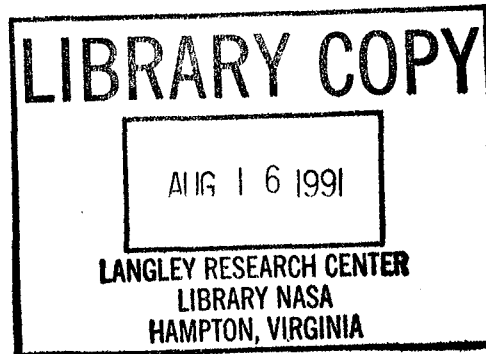
**Experimental Characterization of the  
Perceptron Laser Rangefinder**

**In So Kweon, Regis Hoffman, and Eric Krotkov**

**CMU-RI-TR-91-1**

The Robotics Institute  
Carnegie Mellon University  
Pittsburgh, Pennsylvania 15213

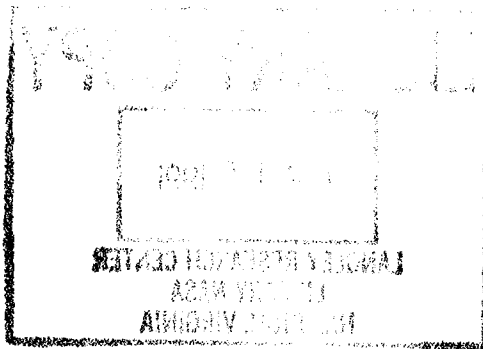
January 1991



©1991 Carnegie Mellon University

This research was sponsored by the National Aeronautics and Space Administration under Grant NAGW-1175. The views and conclusions contained in this document are those of the authors and should not be interpreted as representing the official policies, either expressed or implied, of the funding agencies.

N91-27554 #



# Contents

|          |                                                        |           |
|----------|--------------------------------------------------------|-----------|
| <b>1</b> | <b>Introduction</b>                                    | <b>1</b>  |
| <b>2</b> | <b>The Perceptron Scanner</b>                          | <b>3</b>  |
| 2.1      | Principle of Operation . . . . .                       | 4         |
| 2.2      | Operating Characteristics . . . . .                    | 5         |
| <b>3</b> | <b>Experimental Objectives and Setup</b>               | <b>7</b>  |
| <b>4</b> | <b>Geometric Parameters</b>                            | <b>9</b>  |
| 4.1      | Origin . . . . .                                       | 9         |
| 4.2      | Horizontal Field of View . . . . .                     | 10        |
| 4.3      | Vertical Field of View . . . . .                       | 11        |
| <b>5</b> | <b>Qualitative Characterization</b>                    | <b>14</b> |
| 5.1      | Internal Reflections . . . . .                         | 14        |
| 5.2      | Shadows . . . . .                                      | 15        |
| 5.3      | Skewed Objects . . . . .                               | 16        |
| 5.4      | Vignette Effect . . . . .                              | 16        |
| 5.5      | Frame Rate . . . . .                                   | 18        |
| 5.6      | Mixed Pixels . . . . .                                 | 18        |
| 5.7      | Range Drift . . . . .                                  | 19        |
| <b>6</b> | <b>Statistical Characterization</b>                    | <b>22</b> |
| 6.1      | Angular Resolution . . . . .                           | 22        |
| 6.2      | Precision . . . . .                                    | 24        |
| 6.2.1    | Precision of Pixel Position . . . . .                  | 24        |
| 6.2.2    | Precision of Range Measurements . . . . .              | 25        |
| 6.3      | Accuracy . . . . .                                     | 30        |
| <b>7</b> | <b>Image Processing</b>                                | <b>33</b> |
| 7.1      | Internal Reflections and Vignette Correction . . . . . | 33        |
| 7.2      | Surface Material Correction . . . . .                  | 33        |
| 7.3      | Minimizing Statistical Variations . . . . .            | 35        |

|                              |           |
|------------------------------|-----------|
| <b>8 Discussion</b>          | <b>37</b> |
| <b>A Auto-zero Circuitry</b> | <b>39</b> |
| <b>Acknowledgements</b>      | <b>42</b> |
| <b>References</b>            | <b>43</b> |

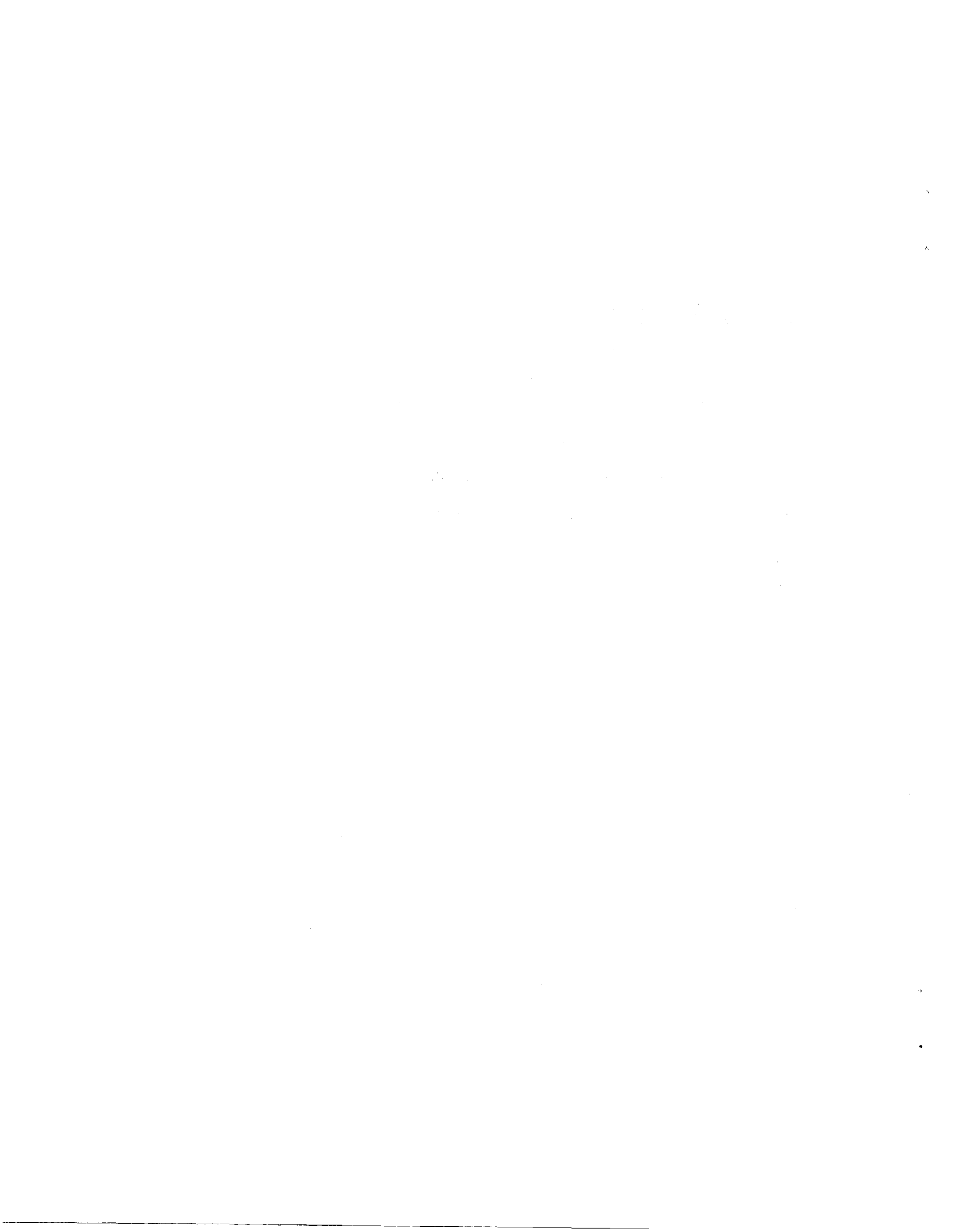
# List of Figures

|      |                                                                             |    |
|------|-----------------------------------------------------------------------------|----|
| 2.1  | The Perceptron scanner. . . . .                                             | 3  |
| 2.2  | Range and reflectance image pair. . . . .                                   | 4  |
| 3.1  | Black target on stand. . . . .                                              | 8  |
| 4.1  | Lines of sight intersect at scanner origin. . . . .                         | 10 |
| 4.2  | Identification of the horizontal field of view. . . . .                     | 11 |
| 5.1  | Two hot spots in image. . . . .                                             | 14 |
| 5.2  | Image smudge due to internal reflection. . . . .                            | 15 |
| 5.3  | Shadows to right of high reflectance objects. . . . .                       | 16 |
| 5.4  | Skewed rectangle in the top portion of the image. . . . .                   | 16 |
| 5.5  | Scanner aperture effect in lower corners of image. . . . .                  | 17 |
| 5.6  | Effect of Frame Rate on Range Measurement. . . . .                          | 18 |
| 5.7  | Mixed pixel effect setup. . . . .                                           | 19 |
| 5.8  | Mixed pixels along horizontal boundary. . . . .                             | 20 |
| 5.9  | Range values drift over time. . . . .                                       | 20 |
| 5.10 | Range values drift due to ambient temperature. . . . .                      | 21 |
| 6.1  | Setup to determine angular resolution. . . . .                              | 23 |
| 6.2  | Range and reflectance statistics across a row in the image. . . . .         | 23 |
| 6.3  | Temporal pixel stability across image. . . . .                              | 24 |
| 6.4  | Range precision under different lighting conditions. . . . .                | 25 |
| 6.5  | Range measurements differ across surface boundaries. . . . .                | 26 |
| 6.6  | Range measurement statistics for different surface materials. . . . .       | 27 |
| 6.7  | The mean of range measurements for different beam incidence angles. . . . . | 28 |
| 6.8  | Standard deviation for different beam incidence angles. . . . .             | 29 |
| 6.9  | Range measurement statistics as temperature increases. . . . .              | 30 |
| 6.10 | Sensor accuracy for different materials. . . . .                            | 32 |
| 7.1  | Range image and result of threshold operation. . . . .                      | 34 |
| 7.2  | Range image and connected regions. . . . .                                  | 34 |
| 7.3  | Range image and valid pixel mask. . . . .                                   | 35 |
| A.1  | Testing the effect of surface material on range measurements. . . . .       | 40 |

**A.2 Mean and standard deviation of range measurements across object boundaries. . . 40**

# List of Tables

|     |                                                           |    |
|-----|-----------------------------------------------------------|----|
| 2.1 | Nominal values of sensor parameters. . . . .              | 5  |
| 4.1 | Vertical field of view results. . . . .                   | 12 |
| 6.1 | A line fit for computing the standoff distance. . . . .   | 31 |
| 7.1 | Comparison of spatial versus temporal variations. . . . . | 36 |



## Abstract

In this report, we characterize experimentally a scanning laser rangefinder that employs active sensing to acquire three-dimensional images. We present experimental techniques applicable to a wide variety of laser scanners, and document the results of applying them to a device manufactured by Perceptron. Nominally, the sensor acquires data over a  $60^\circ \times 60^\circ$  field of view in  $256 \times 256$  pixel images at 2Hz. It digitizes both range and reflectance pixels to 12 bits, providing a maximum range of 40m and a depth resolution of 1cm.

We present methods and results from experiments to measure geometric parameters including the field of view, angular scanning increments, and minimum sensing distance. We characterize qualitatively problems caused by implementation flaws, including internal reflections and range drift over time, and problems caused by inherent limitations of the rangefinding technology, including sensitivity to ambient light and surface material. We characterize statistically the precision and accuracy of the range measurements.

We conclude that the performance of the Perceptron scanner does not compare favorably with the nominal performance, that scanner modifications are required, and that further experimentation must be conducted.



# Chapter 1

## Introduction

Many tasks and problems require three-dimensional information about the environment. For example, mobile robot navigation systems require this information to avoid obstacles, and to achieve high-speed mobility [6]. Similarly, the performance of object recognition systems improves dramatically given three-dimensional data [3].

A rich variety of passive vision techniques produce three-dimensional information [8]. Traditionally, they have lacked robustness and generality, and have not proven themselves effective in practice. Passive stereo vision is a particularly promising source of range information, but requires substantial data processing to match images with each other and to determine range by triangulation.

Active sensing techniques promise to simplify many tasks and problems in machine vision [7]. Active sensors transmit some form of energy into the environment, and sense the reflected signals; examples include radar, sonar, structured light, and scanning laser rangefinders. Active sensing techniques can provide range data with less computation, and can be relatively insensitive to illumination conditions (e.g., they can operate at night).

Several authors have surveyed the active sensing research conducted by the robotics and vision communities. Jain and Jain [7] report on emerging themes and research issues in the analysis and interpretation of range images, and present a comprehensive bibliography. Besl [2] examines a wide variety of range imaging technologies, and compares them quantitatively by evaluating a figure of merit based on range accuracy, depth of field, and image acquisition time. Everett [4] surveys collision avoidance and ranging sensors for mobile robots. Nitzan [9] assessed range sensors for diverse robotic applications,

From these surveys and our own observations, we perceive both a great potential for active sensing technology, and a relative lack of practical experience with it on the part of robotics and machine vision researchers. Consequently, we set out to study one particular active sensor, a scanning laser rangefinder manufactured by Perceptron, which we employ currently in our research on mobile robot navigation systems [1, 12].

A number of researchers [5, 13] have studied a very similar sensor manufactured by Erim [15]. Because these papers concentrate on larger problems in robot navigation, they omit (rightfully) many practical details and results concerning the sensor, and do not address at all some important

implementation topics. We intend to focus on the practical details (in the spirit of Watts et al. [14]), and to address topics of practical consequence that have received little or no attention to date. For the purposes of this report, our specific objective is to examine experimentally the Perceptron scanner's performance by conducting experiments to identify its geometric, qualitative, and statistical characteristics. As part of this effort, we aim to develop methods to identify sensor parameters and techniques to determine whether the sensor is operating correctly.

We report our methods and findings as follows. Chapter 2 discusses the principle of operation and the nominal operating characteristics of the scanner. Chapter 3 outlines the experimental objectives and setup, and Chapter 4 defines the geometric parameters related to scanning mechanism. The next two chapters address the radiometric parameters related to the electronics and optics of the sensor. Chapter 5 examines the qualities we observe about the images, such as image hot spots and skewing of the scene. Chapter 6 looks at statistical measures of the image, including drift over time, and image stability. Chapter 7 discusses some of the image processing techniques we have implemented to compensate for deficiencies of the scanner, and Chapter 8 concludes the report by summarizing its findings.

## Chapter 2

# The Perceptron Scanner

The Perceptron scanning laser rangefinder is an optical-wavelength radar system<sup>1</sup>, and is comparable to devices built by Erim [15] and Odetics [10]. The sensor volume is roughly  $50 \times 45 \times 35$ cc and the mass is about 30kg (Figure 2.1). This section outlines the theory of operation of the scanner, describes its major features, and defines a number of its geometric and radiometric parameters.

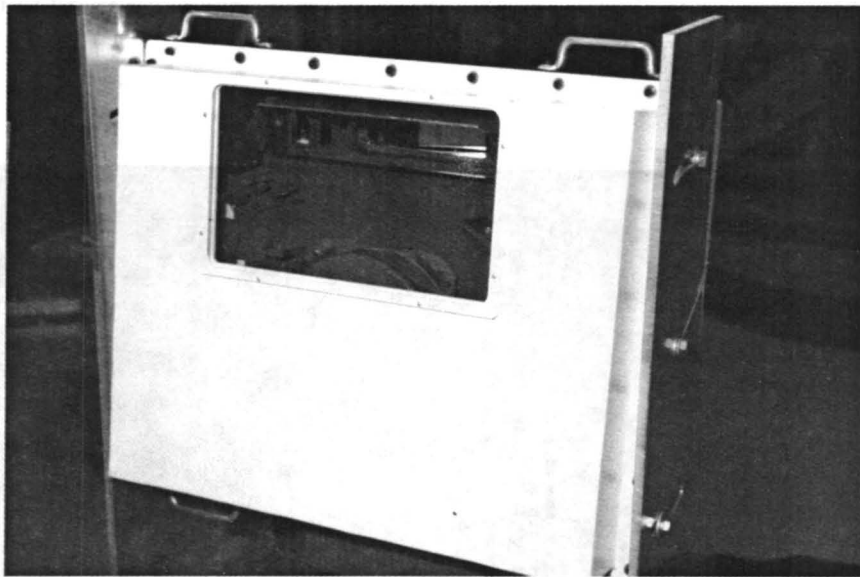


Figure 2.1: The Perceptron scanner.

---

<sup>1</sup>Optical radar is also called Lidar, which is an acronym for Light Detection And Ranging.

## 2.1 Principle of Operation

The Perceptron scanner operates by sweeping a laser beam across the field of view. A nodding mirror changes (tilts) the elevation of the transmitted signal and a hexagonal mirror changes (pans) the azimuth. The laser beam is generated by an amplitude modulated laser diode that emits 180mW of laser power at 810nm (near-infrared). Varying the drive current to the diode modulates the amplitude of the laser light.

A surface in the environment reflects the laser beam back toward the scanner, where receiver optics focus it onto an avalanche photodiode. After filtering, an electronic detector measures the difference in phase between the transmitted and received signals. The phase difference is proportional to the transit time, and therefore the distance (range) traveled by the laser beam. A final circuit, implemented as a lookup table, compensates the computed range for variations in reflected energy due to different surface materials.

The scanner forms two images, neither in the optical sense. The image in Figure 2.2 from our robot test course consists of several large rocks in the foreground, a sand-covered floor, and several boxes scattered in the background. In the *range image* (the left-hand side of Figure 2.2), the pixel values correspond to the range determined by phase differences of the amplitude modulated signals. In the *reflectance image* (the right-hand side of Figure 2.2), the pixel values correspond to the magnitude of laser energy reflected. In both, the pixel positions correspond to the laser beam direction defined by the mirror angles.



Figure 2.2: Range and reflectance image pair.

Phase differences can be determined only modulo  $2\pi$ . Therefore, an inherent limitation of this principle of operation is that it cannot measure range uniquely, i.e., it measures range only to within

an *ambiguity interval*. External constraints (not discussed here) must be employed to resolve that ambiguity.

## 2.2 Operating Characteristics

Table 2.1 summarizes the operating characteristics of the sensor as specified by the manufacturer [11]. We discuss these in the order given in the table.

| Parameter       | Units | Value | Description                    |
|-----------------|-------|-------|--------------------------------|
| $\phi_{fov}$    | deg   | 60    | Vertical FOV                   |
| $\theta_{fov}$  | deg   | 60    | Horizontal FOV                 |
| $N_{rows}$      | pixel | 256   | Number of rows                 |
| $N_{cols}$      | pixel | 256   | Number of columns              |
| $\Delta_\phi$   | deg   | 0.24  | Vertical angle increment       |
| $\Delta_\theta$ | deg   | 0.24  | Horizontal angle increment     |
| $R_{ambig}$     | m     | 40    | Ambiguity interval             |
| $N_{range}$     | bit   | 12    | Number of bits for range       |
| $N_{ref}$       | bit   | 12    | Number of bits for reflectance |
| $\Delta_R$      | cm    | 0.98  | Range quantization error       |

Table 2.1: Nominal values of sensor parameters.

To define the parameters related to the scanning geometry, let  $\phi$  and  $\theta$  denote the angular orientations of the nodding and hexagonal mirrors, respectively. Let  $\phi_s$  and  $\theta_s$  be the start angles of the two mirrors, and  $\phi_f$  and  $\theta_f$  the final or end angles. Then the vertical field of view is  $\phi_{fov} = \phi_f - \phi_s$ , and the horizontal field of view is  $\theta_{fov} = \theta_f - \theta_s$ .

Image formation quantizes space by mapping the entire scene to an array of points. Let  $N_{rows}$  be the number of rows in the image and  $N_{cols}$  the number of columns. Assuming that the mirrors scan uniformly (equal angles), each angular increment of the nodding mirror is  $\Delta_\phi = \frac{\phi_{fov}}{N_{rows}-1}$ , and each angular increment of the hexagonal mirror is  $\Delta_\theta = \frac{\theta_{fov}}{N_{cols}-1}$ .

Image formation also quantizes depth. Let the number of bits in a range measurement be  $N_{range}$ , and let  $R_{ambig}$  be the ambiguity interval caused by the phase change  $2\pi$ . Then it follows that the range quantization error is  $\Delta_R = \frac{R_{ambig}}{2^{N_{range}-1}}$ .

The size of the laser beam is another characteristic of the scanner. We call the intersection of the beam with a surface the laser *footprint*. Suppose that one particular laser beam strikes a surface depth discontinuity. Then object surfaces at multiple distances will reflect the laser signal, resulting in a phase difference measurement that is not unique and not necessarily meaningful. This corrupts the range measurement at the pixel, giving rise to the *mixed pixel* problem. Mixed pixels occur only near object edges.

Another factor bearing on the mixed pixel problem is beam divergence, or imperfect collimation, due to diffraction effects in the projector telescope. Beam divergence causes the diameter of the beam to grow from 17mm as it exits the projector telescope to approximately 50mm at 40m [11]. The larger the beam divergence, the larger the laser footprint, and consequently, the more severe is the mixed pixel problem.

# Chapter 3

## Experimental Objectives and Setup

Our experimental objectives are to characterize the scanner and to identify its geometric and radiometric parameters. We answer the following questions about sensor performance:

### Geometry

- Field of view.
- Minimum distance. We call the minimum distance the *offset* distance. This is the actual distance corresponding to a range measurement of zero.

### Radiometry

- Accuracy. What is the difference between computed range and true range? Does the accuracy depend on target distance? Are there systematic errors?
- Precision. Does a static object point project to the same pixel over time? Does the measured depth of static object point vary over time?
- Depth resolution. What is the minimum detectable depth change as a function of target distance? We distinguish depth resolution (just noticeable difference) from depth quantization.
- Angular resolution. What is the minimum detectable width or height of a target?

### Performance

- Distance. Do range measurements depend significantly on object distance?
- Ambient light. Do illumination conditions affect range or reflectance measurements?
- Surface material. For two objects at the same distance from the scanner but with different surface materials, do the range measurements differ?
- Temperature. Do range measurements depend significantly on ambient temperature?
- Incidence angle. How does beam incidence effect the range measurement?

We conduct the experiments inside a 30m × 20m building (highbay). The area has both natural illumination that enters through windows, and artificial illumination generated by lamps mounted on the ceiling. We will refer to these lamps as *spotlights* because they are powerful and somewhat directional.

We mount the scanner about 80cm above the floor on a table. We can move a target mounted on a stand within the building (Figure 3.1). The stand allows us to adjust the height of the target and to rotate the target about a vertical axis. (The rotational degree of freedom will be useful for studying the effects of different beam incidence angles.)

We can mount different targets on the stand. One family of targets consists of planar, cardboard slabs of dimension 61cm × 53cm. One target is untreated, another is coated with soil, another has gravel chips glued to it, a fourth is painted black. The different surface materials exhibit different reflectance properties, which range from strong (untreated) to weak (black paint).

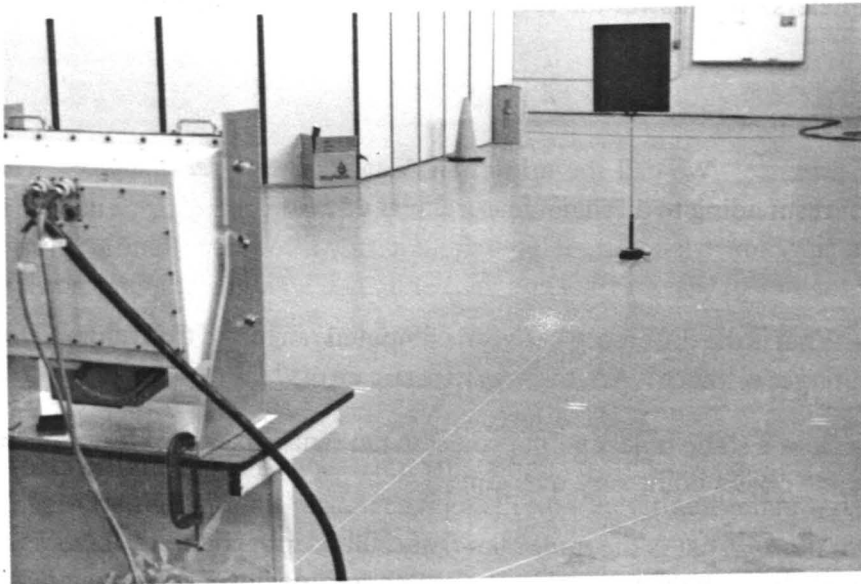


Figure 3.1: Black target on stand.

# Chapter 4

## Geometric Parameters

We measure sensor parameters relevant to the geometry of the scanner. Those parameters are the origin, the field of view, and the angle increments.

### 4.1 Origin

This section describes a graphical method to identify the geometric origin of the scanner in two dimensions, and presents results from one trial. Assuming a flat floor in the experimental area, the method is as follows (Figure 4.1).

1. Adjust the stand so that the target is the same height as the scanner (80cm). As we move the target to different positions, it remains at the same height as the scanner, because the floor is reasonably flat.
2. Tilt the scanner until the center of the target projects to row 127 in the reflectance image.
3. Position the target about 6m from the scanner, so that the target center projects to column 127 in the reflectance image.
  - (a) Move the target 2m away from the scanner (radially) so that the target still projects to column 127.
  - (b) Mark the floor where the target stands.
  - (c) Repeat steps (a) and (b) a total of six times. Thus, the final target position lies about 16m from the scanner.
  - (d) Draw a line on the floor connecting the marks. Because this line appears as the center column of the image, we will call it the *vertical line*.
4. Repeat step 3 for columns 0 and 255.

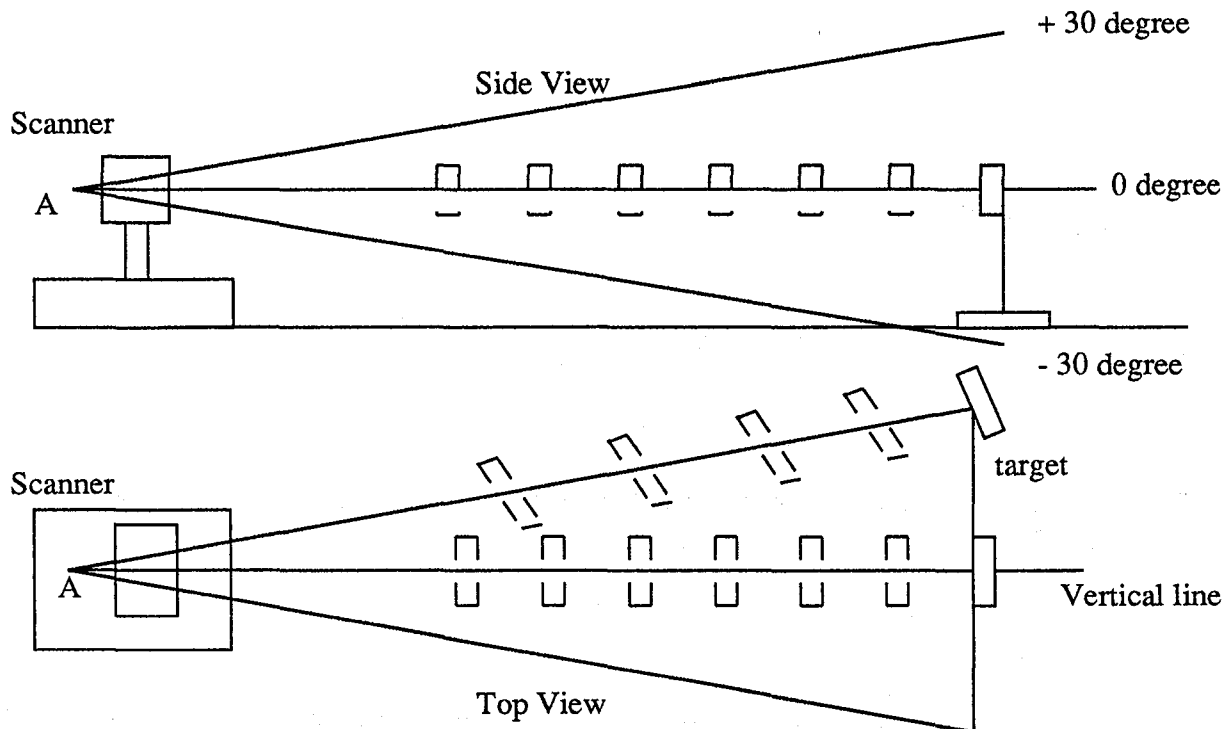


Figure 4.1: Lines of sight intersect at scanner origin.

This procedure produces three lines drawn on the floor. Their intersection (point A in Figure 4.1) is the projection of the scanner origin onto the floor. As the figure shows, the origin lies outside the scanner, several centimeters behind the rear surface of the housing.

The lines do not intersect exactly at a point. Instead, they form a triangle, whose largest cross section is approximately 5cm. One possible cause of this deviation from the ideal is that the center of the target does not project to row 127 in all cases, as required in step 2. Instead, we find that the image coordinates of the target shift, typically one or two pixels, as we move the target. The reason for this may be that the floor is not perfectly flat.

Although two lines suffice to define the origin, we draw three because more data increases the robustness of the procedure. Further, choosing in step 4 the extreme column coordinates helps delimit the horizontal field of view (see Section 4.2).

Having identified and marked the origin, we secure the end of a tape measure to point A, and extend the tape into the scene along the vertical line. This defines a “ground truth,” allowing us to compare computed range values with distance measurements read from the tape measure.

## 4.2 Horizontal Field of View

To measure the horizontal field of view, we place two targets so that they are visible in the first and last column in the image ( $i$  and  $j$  in Figure 4.2). As in the previous section, the targets are at the

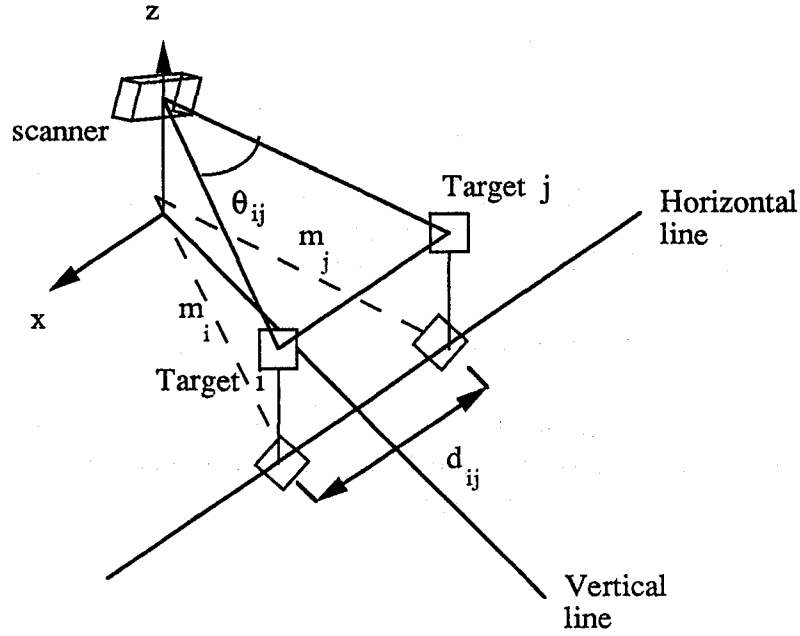


Figure 4.2: Identification of the horizontal field of view.

same height as the scanner and each other. The (fictional) line joining the two targets, and the laser beams passing through them form a triangle parallel to the floor. From this triangle and the law of cosines, we compute the angle between the two targets by

$$\theta_{ij} = \arccos \left( \frac{d_{ij}^2 - m_i^2 - m_j^2}{2m_i m_j} \right) \quad (4.1)$$

where  $m_i$  and  $m_j$  are the distances from the origin to the two targets, and  $d_{ij}$  is the distance between them (we measure all distances manually on the ground plane). Because the targets lie at the extremes of the horizontal field of view,  $\theta_{fov} = \theta_{ij}$ . Assuming that the horizontal angular increments are equal, we can compute the horizontal angle increment from  $\theta_{fov}$  by

$$\Delta_\theta = \frac{\theta_{fov}}{N_{cols} - 1} \quad (4.2)$$

The experiment resulted in a horizontal field of view  $\theta_{fov} = 60.3^\circ$  and  $\Delta_\theta = 0.236^\circ$ . This compares with a stated horizontal field of view of  $60^\circ$  and  $\Delta_\theta = 0.235^\circ$ .

### 4.3 Vertical Field of View

Several different experiments measure the vertical field of view and angle increment. Table 4.1 summarizes the results, which we discuss below.

| Method                      | Vertical Angle Increment | Vertical FOV |
|-----------------------------|--------------------------|--------------|
| Tilting Scanner             | 0.1667 deg.              | 42.50 deg.   |
| Using a Plumb Line          | 0.1566 deg.              | 39.93 deg.   |
| Using the Programmable Tilt | 0.2083 deg.              | 53.12 deg.   |

Table 4.1: Vertical field of view results.

A notable result is that the vertical field of view is not near the stated value of  $60^\circ$ . In discussions with the manufacturer, it was discovered that an incorrect constant in the scanner control software caused this. Perceptron adjusted their software to correct this.

### Tilting the Scanner

We place the target on the vertical line and take an image. We physically tilt the scanner about the scanner mount axis and take another image. Between images, the target appears to shift along the center column. We measure the difference  $\Delta r$  in row coordinates of the same target point. We measure with a protractor the change  $\Delta tilt$  in the tilt angle. The vertical angle increment and the field of view are given by

$$\Delta_\phi = \frac{\Delta tilt}{\Delta r} \quad (4.3)$$

$$\phi_{fov} = \Delta_\phi (N_{rows} - 1) \quad (4.4)$$

The result value of  $\phi_{fov} = 42.5^\circ$ .

### Using a Plumb Line

We place three equidistant marks along a plumb line, and suspend it from the target stand. Let  $h$  be the distance between the marks. We position the stand so that all the marks appear along column 127 of the reflectance image, and the center mark appears at row 127.

We measure manually the distance  $d$  from the origin to the target. The angle subtended by two marks is  $\Delta tilt = \tan \frac{h}{d}$ . From a reflectance image, we compute the difference  $\Delta r$  between the row coordinates of the projections of the marks.

With  $\Delta tilt$  and  $\Delta r$  we compute the vertical angle increment by Equation (4.4) and the vertical field of view by Equation (4.4). The result value of  $\phi_{fov} = 39.93^\circ$ .

### Programming the Tilt Angle

We draw a line on the floor that projects to one row of the image. We change the vertical field of view in increments of  $\Delta = 5^\circ$  by programming the scanner. As we tilt the field of view, we count the number of rows  $S$  that the projection of the line shifts.

We find that the vertical angle increment is

$$\Delta_{\phi} = \frac{\Delta}{S} = \frac{5^{\circ}}{24 \text{ rows}} = \frac{0.2083^{\circ}}{\text{row}} \quad (4.5)$$

The result value of  $\phi_{fov} = 53.12^{\circ}$ . The error resulting from the programmable tilt mechanism may be due to the imprecise starting position of the nodding mirror and incorrect mirror control constants supplied by the manufacturer. In other words, even though we instructed the scanner to change its field of view, we are not sure whether the scan will start at the same angular position. Therefore, the actual angle increment may not correspond to the field of view change as instructed by the programmable tilt mechanism.

### Remarks

In retrospect, physically tilting the scanner yields the worst measurements. This is due to difficulty in accurately measuring the scanner tilt angle. Another problem is that the scanner is rotated about its mount axis, which is not necessarily the axis of the scanner.

# Chapter 5

## Qualitative Characterization

Many sensor characteristics can be noted by observing the images both spatially and temporally. This section discusses several aspects of the sensor images that caused problems.

### 5.1 Internal Reflections

We observe two holes or hot spots in the range and reflectance images. These appear as two white blobs in the upper center of the images in Figure 5.1. These are believed to be due to interreflections within the Perceptron scanner.

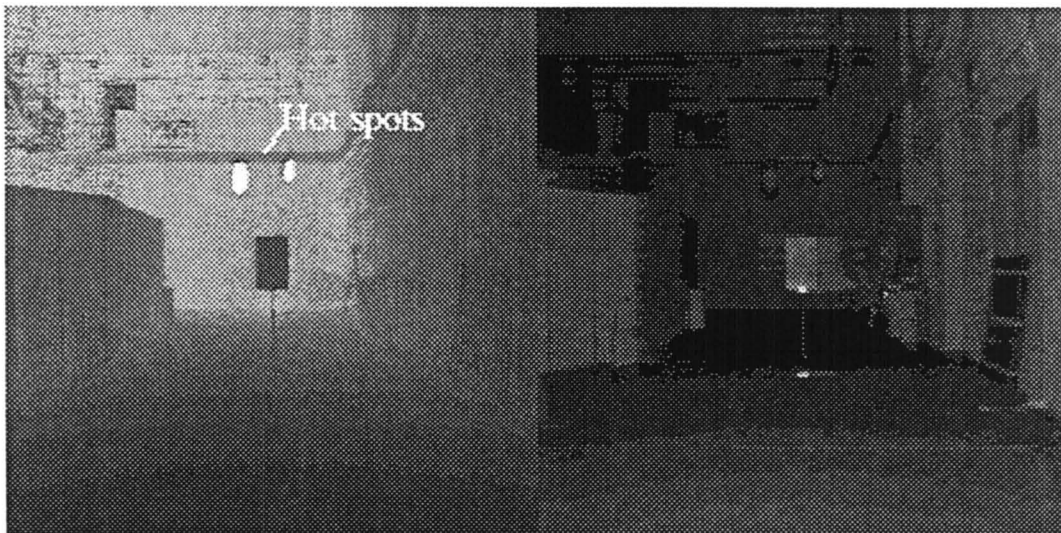


Figure 5.1: Two hot spots in image.

Figure 5.2 shows the effect of a scanner internal reflection on the image. The highlighted area in the range image consists of a flat floor. However, magnifying the region (shown in the right-hand side of Figure 5.2) shows that the range values are not constant. We have observed variations of 40-50 range counts within this region. This "smudge" is always located at the same position in the image (regardless of sensor orientation). Removal of the sensor exit window eliminates the smudge, so we conclude that some internal reflections (reflections of the laser beam off the exit window) lead to this problem.

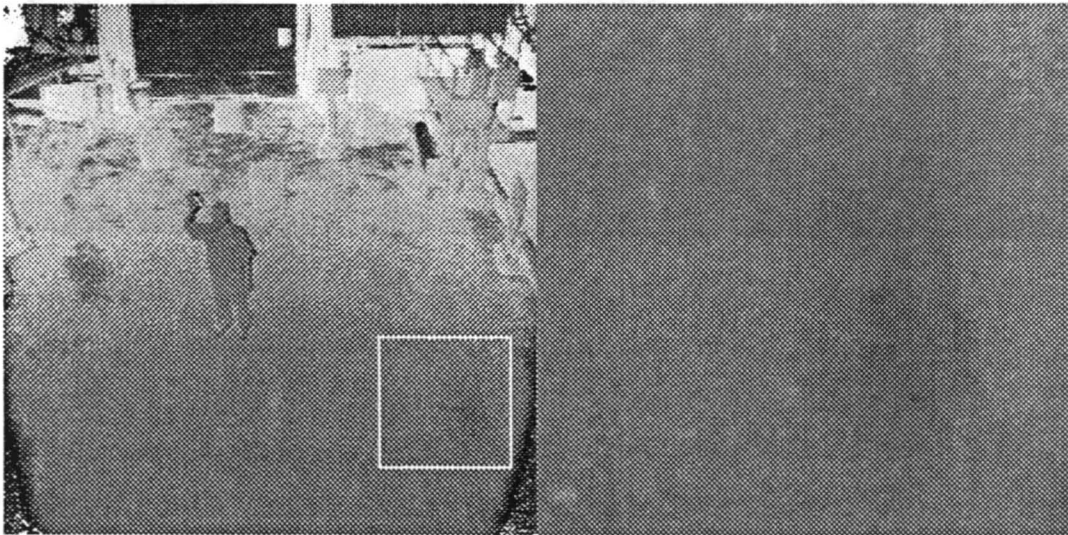


Figure 5.2: Image smudge due to internal reflection.

Range image on left, magnified region on right.

## 5.2 Shadows

We observe shadows to the right of high-reflectance objects (Figure 5.3). In the figure, the area to the immediate right of the large, white cardboard target has a shadow in the reflectance image. As the laser beam scans from left to right across the scene, we believe that this effect is due to the avalanche photodiode not being completely discharged, and hence having a "memory" of previous pixels along the scan line.

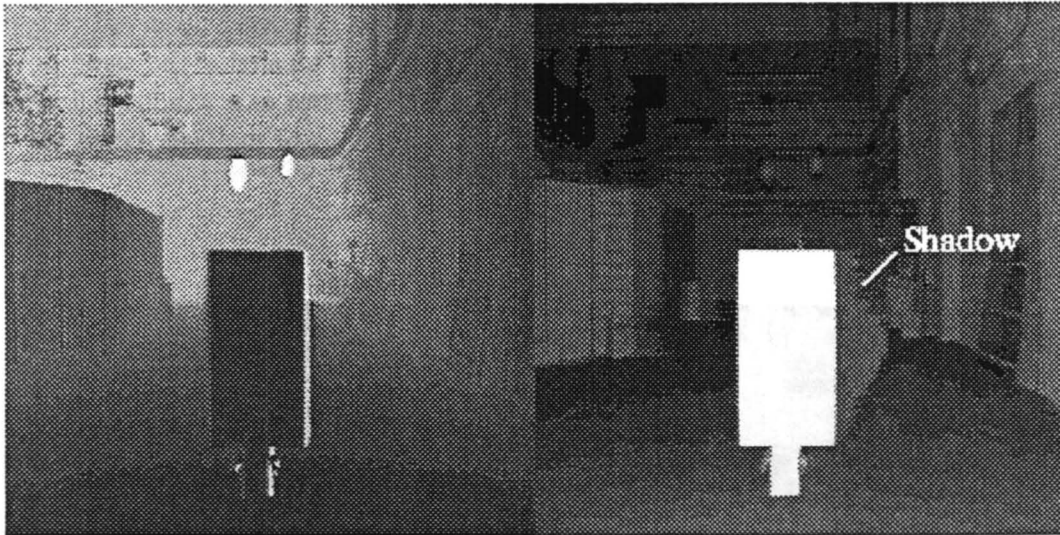


Figure 5.3: Shadows to right of high reflectance objects.

### 5.3 Skewed Objects

Although the target was a perfect rectangle on a vertical wall, we observed a skewed rectangle in the top of the image (e.g., see the skewed rectangle in the intensity image of Figure 5.4). The wire-frame model (black rectangle in the intensity image) shows the correct projection of the rectangle. This may be due to the fact that the nodding mirror is still accelerating when it starts scanning. Once the mirror reaches a terminal velocity, we do not observe any more skew.

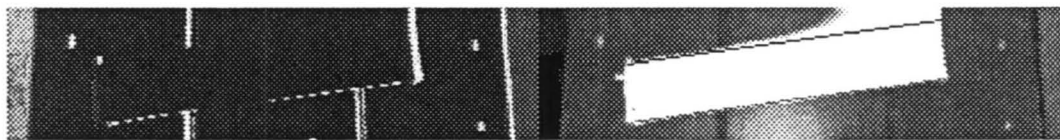


Figure 5.4: Skewed rectangle in the top portion of the image.

### 5.4 Vignette Effect

The aperture of the scanner causes problems at the bottom of images. The lower corners of Figure 5.5 have a vignette or region where the pixel values are incorrect.



Figure 5.5: Scanner aperture effect in lower corners of image.

Range image on left, magnified region on right.

## 5.5 Frame Rate

The stated frame rate of the scanner is 2 Hz, or a range/reflectance image pair every 0.5 seconds. However, when taking images at this rate, we observed that not all images of a static scene appeared identical. A series of say 20 images would be the same, the next image would be noticeably lighter (i.e. have higher range values), then the next series would be the same as the initial sequence. This temporal problem diminished as the frame rate decreased. An experiment that tabulated the range measurement at a specific target point while the frame rate increased is summarized in Figure 5.6. A trial consisted of taking a range measurement of a fixed target, waiting  $n$  seconds ( $n$  an integer), then repeating 100 times to obtain a mean range measurement. The experiment was then repeated for a different delay  $n$ . The range measurement does not stabilize until frame rates are less than 0.5 Hz. It is not clear what causes this phenomenon.

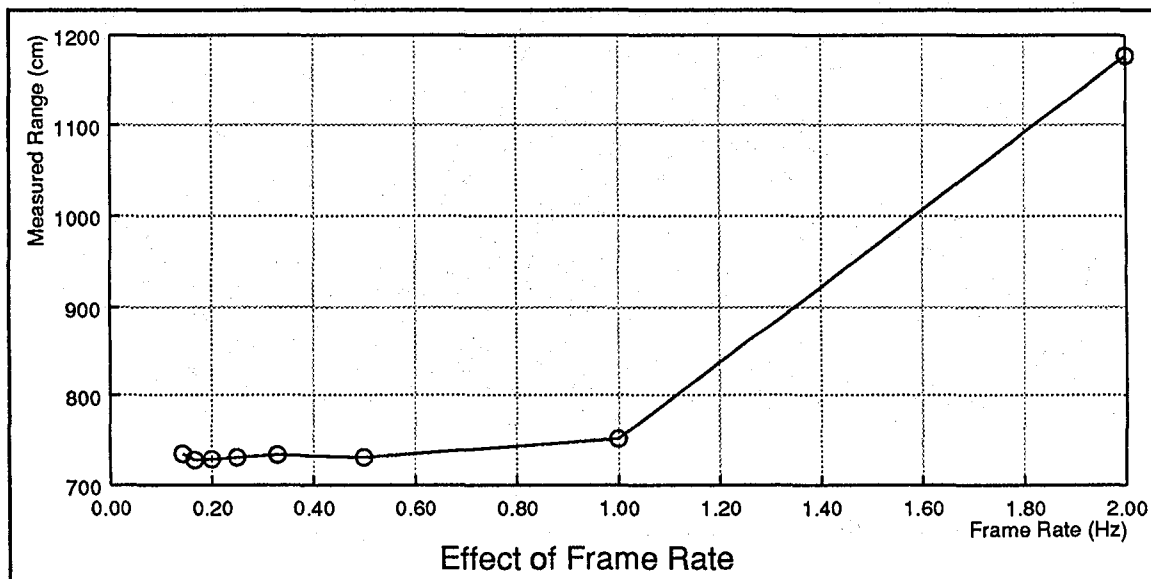


Figure 5.6: Effect of Frame Rate on Range Measurement.

## 5.6 Mixed Pixels

Mixed pixel refers to a pixel which lies on the edge of an object and therefore has a range value that is a combination of the range value of the background and the range value of the object (due to the finite size of the laser footprint). An experiment to examine this effect is shown in Figure 5.7. Here the foreground target is a small piece of cardboard, with a larger cardboard background.

Because it is difficult to see the mixed pixel effect in the image, we plot measured range values along columns of the top horizontal boundary of the foreground target (see Figure 5.8).



Figure 5.7: Mixed pixel effect setup.

Points represented by a plus lie on the background and points represented by a diamond are on the foreground. At the boundary between the two targets, the range value (represented by a circle), is some combination of the foreground range and background range. In essence, there is no sharp change in the image corresponding to a sharp discontinuity in the scene. Thus, care must be taken when using range values at surface boundaries. In particular, edge detection methods that rely on large range discontinuities must be avoided.

## 5.7 Range Drift

To determine if the range values drift over time, we placed the cardboard target at a fixed distance from the origin of the scanner, and took many images over several hours without moving the target. We observed that range values of a particular pixel drift over time (see Figure 5.9). We placed the cardboard target at a fixed distance 8m from the origin of the scanner and took 10,000 images over a 3 hour period. Figure 5.9 shows the measured range value at one pixel plotted as a function of time (or image number).

Since we observed not a random but a linear drift in range measurements, we hypothesized that the drift might be due to a change in ambient temperature. To confirm this idea, we ran the same experiment under different ambient temperatures. We placed an electric heater behind the scanner to control the ambient temperature.

Figure 5.10 shows range values at a particular pixel point over 14,000 images. Without the heater, we observed approximately constant range measurements between images 0 through 8,100

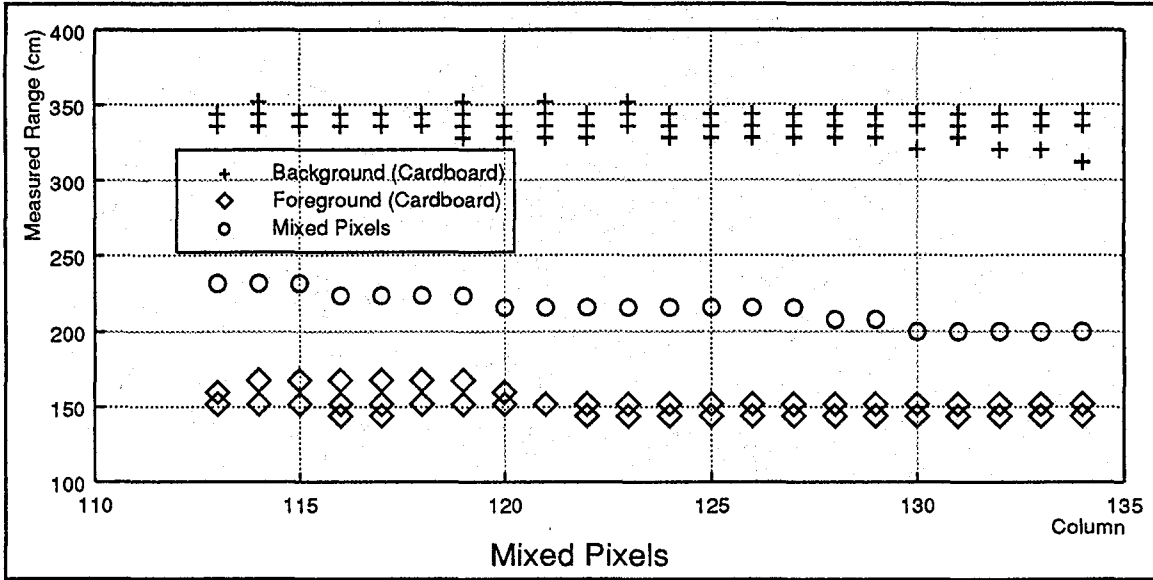


Figure 5.8: Mixed pixels along horizontal boundary.

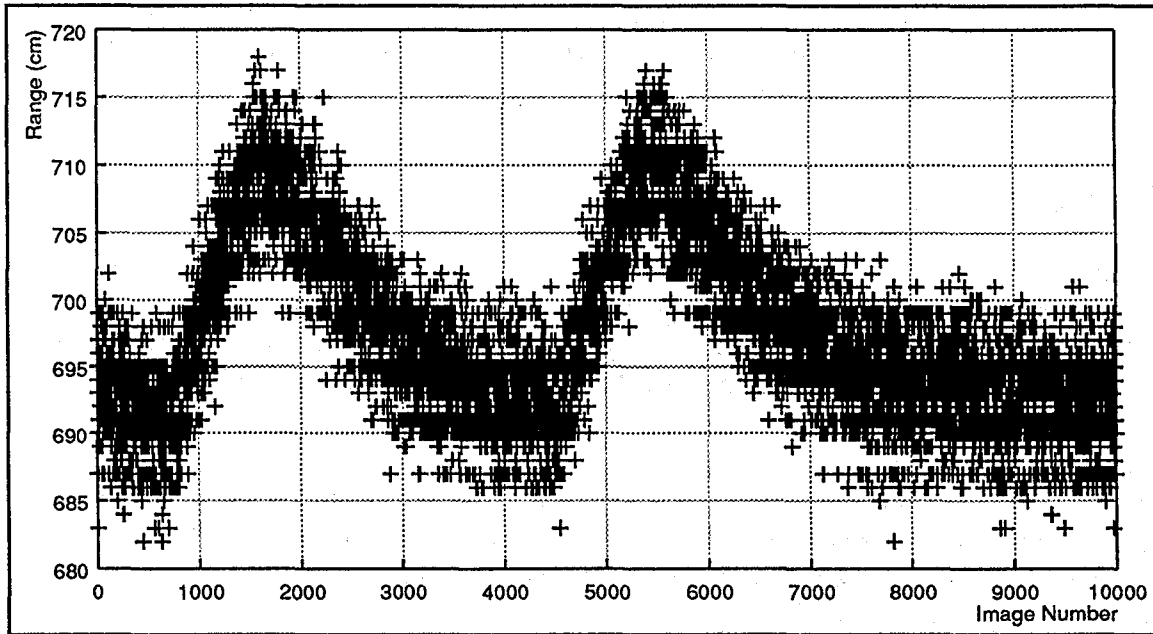


Figure 5.9: Range values drift over time.

(the ambient temperature was  $70^{\circ}F$ ). Then, the heater was turned on, and we waited 30 minutes until the ambient temperature behind the scanner became  $113^{\circ}F$ . We observed an abrupt change in range measurements as shown at time *A* in the figure. While we were continuously taking images, we turned off the heater at time *B* and observed a gradual increase in range measurements. Similarly, we again turned on the heater when the temperature became  $70^{\circ}F$  (at time *C*). As the temperature increased, the range measurements decreased as shown between *C* and *D*. At time *D*, we observed a gradual increase in range measurements as soon as we turned off the heater. This could explain the cyclic nature of the data in Figure 5.9 caused by the building cooling system with a 1 hour period.

We conclude there is both a short term drift in range measurements (of about  $\pm 15\text{cm}$ , seen in images 0 – 8000 in Figure 5.10), and a long term drift associated with ambient temperature. Thus, a range measurement is very sensitive to the ambient temperature.

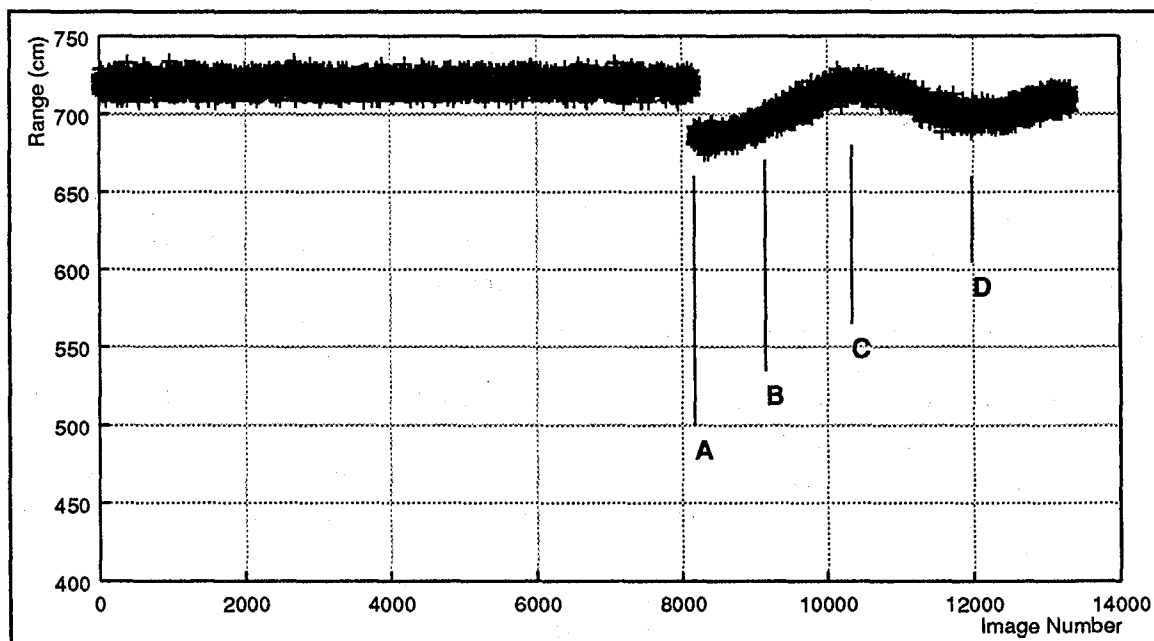


Figure 5.10: Range values drift due to ambient temperature.

# Chapter 6

## Statistical Characterization

This section discusses statistical characteristics of the Perceptron scanner, including angular resolution, precision, and accuracy.

### 6.1 Angular Resolution

The angular resolution of a scanner is a measure of the minimum width an object must be to be detected by the scanner. Instead of directly measuring the minimum detectable width of a target, we use an indirect method based on the fact that the minimum detectable width of the target corresponds to the distance (as measured by the number of columns and denoted by  $\Delta_{column}$  between the target boundary and the portion of the target where the range measurements are approximately constant. Therefore, we can determine the minimum width by observing a sudden change in range measurements along the target boundary.

If the depth change is noticed only at the boundary pixel, the angular resolution and the angular increment are identical. In practice, however, the receiver optics are designed to have a field of view several times larger than the beam size (cf. Section 2.2)

The experimental setup consists of two targets, one small and one large (approximately  $1\text{m} \times 2\text{m}$ ). We place the small target 7m from the scanner, and the large target 2m further (Figure 6.1). The small target appears in the image between columns 121 and 135.

Figure 6.2 shows the mean, over 100 images, of range and reflectance measurements taken along one row. Between columns 123 and 133, we observe a constant depth value of 711 cm. At the object boundaries, we see a sharp change in the mean extending over 2 pixels (from 120 to 122 and from 135 to 137). Therefore, at this particular distance,  $\Delta_{column}$  is 2. The angular resolution  $\Delta_{angle}$  is given by

$$\Delta_{angle} = 2\Delta_{column}\Delta_{\theta} = 0.941^{\circ} \quad , \quad (6.1)$$

where  $\Delta_{\theta}$  is the horizontal angle increment.

We can also estimate the minimum detectable width of an object at a given distance using the resulting  $\Delta_{angle}$ .

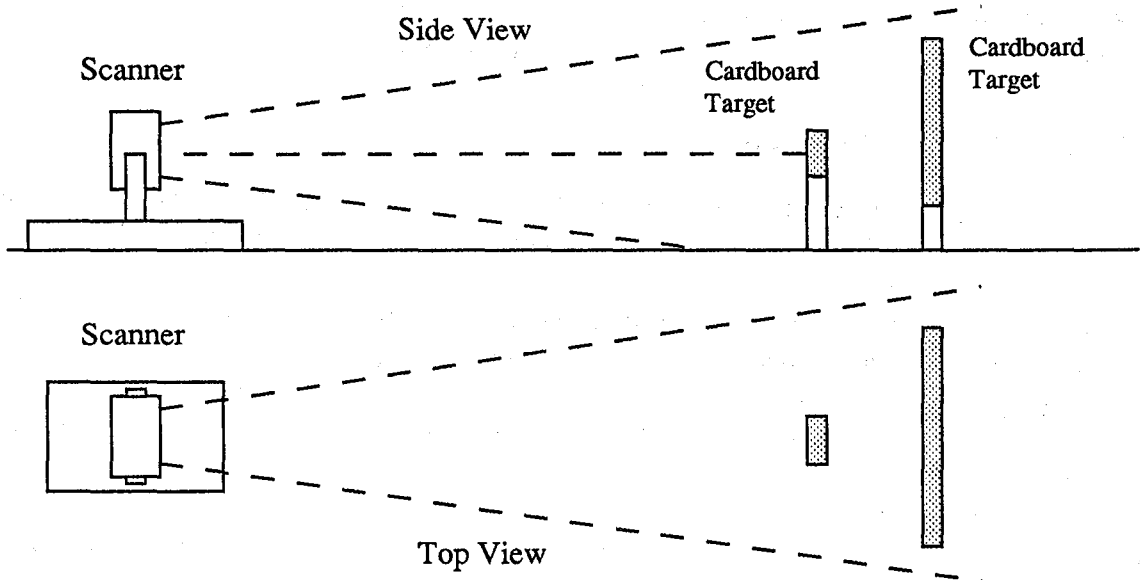


Figure 6.1: Setup to determine angular resolution.

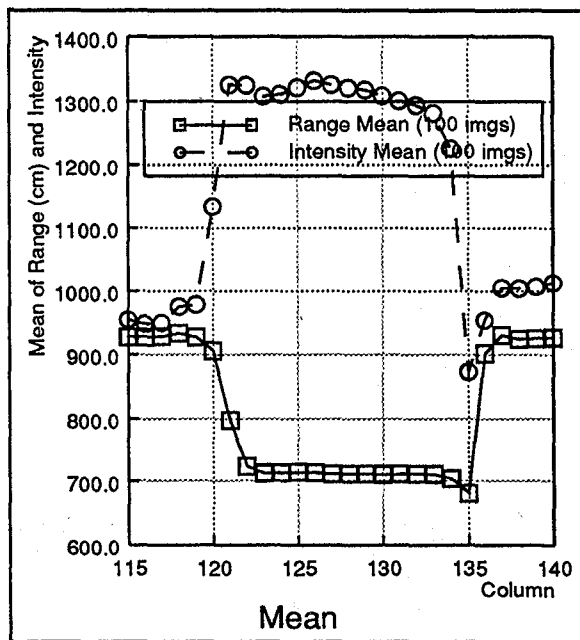


Figure 6.2: Range and reflectance statistics across a row in the image.

## 6.2 Precision

Precision experiments determine how much repeated measurements vary. We investigate the precision of two quantities: pixel position and range measurement.

### 6.2.1 Precision of Pixel Position

To measure the repeatability in pixel position, we take a series of images of the same scene without altering the scanner configuration. We expect a point in the scene to project to the same pixel position over those images.

We position the scanner in front of a vertical wall on which we have drawn white circles (radius 12cm) surrounded by black squares. We consider regions, because we find it difficult to position experimentally a target that maps to only one pixel in the image. We acquire a sequence of images. From each reflectance image we extract the white circle by thresholding, and then compute the centroid of the circular region.

Figure 6.3 plots the standard deviation of the circle centroid positions for several row and column positions. The standard deviation is the order of  $0.025^\circ$  - for comparison, the column angle increment of  $0.24^\circ$  is also plotted. The figure shows that the standard deviation of the centroid varies little over time. It also shows that the standard deviation is an order of magnitude smaller than the nominal horizontal angle increment, and varies little over different pixels in the image.

From this we conclude that, in general, the precision of pixel position is high, and that image stability is independent of pixel position.

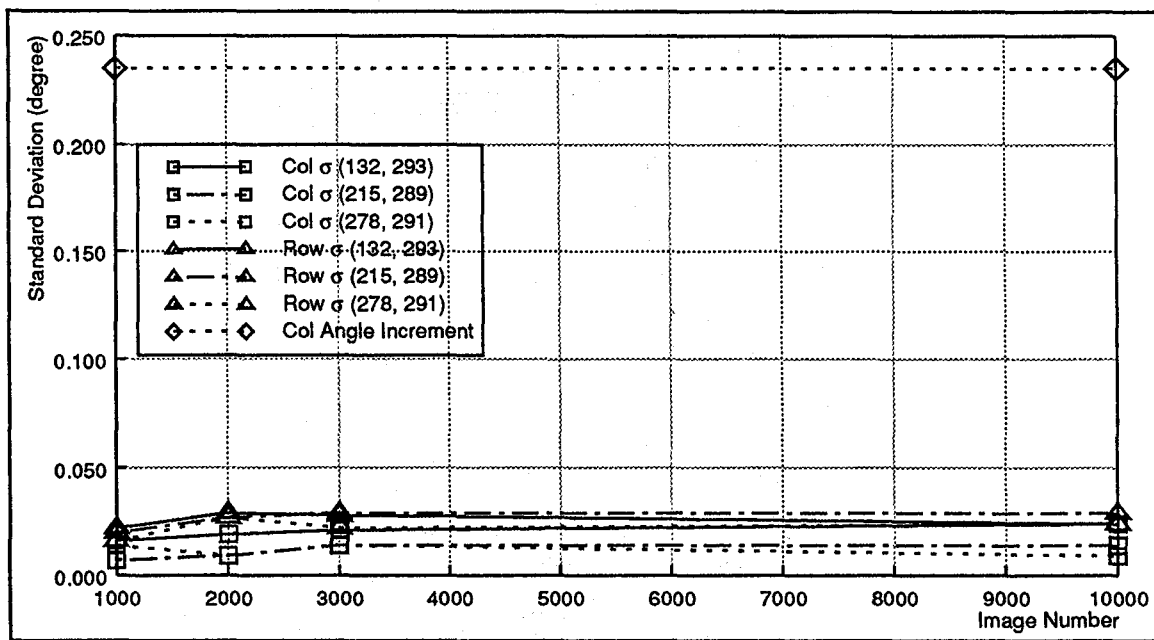


Figure 6.3: Temporal pixel stability across image.

## 6.2.2 Precision of Range Measurements

In this section, we describe experiments to measure the range precision. We vary the ambient light, surface material of the target, distance from the scanner to the target, beam incidence angle at the target, and ambient temperature. Under each of these conditions, we take 100 images at each target position, and compute the mean and variance of the depth measurements.

### Effect of Ambient Light

To study the effect of ambient light on sensed range, we place the black target at one distance, take 100 images, and compute the mean and variance in range at particular pixels. We repeat this procedure for six target distances between 6 and 16m under different indoor lighting conditions: during a sunny day, and during a cloudy day both with and without spotlights.

Figure 6.4 shows that the precision decreases with intensity of illumination. We conclude that the brighter is the ambient light, the more the range measurements vary temporally.

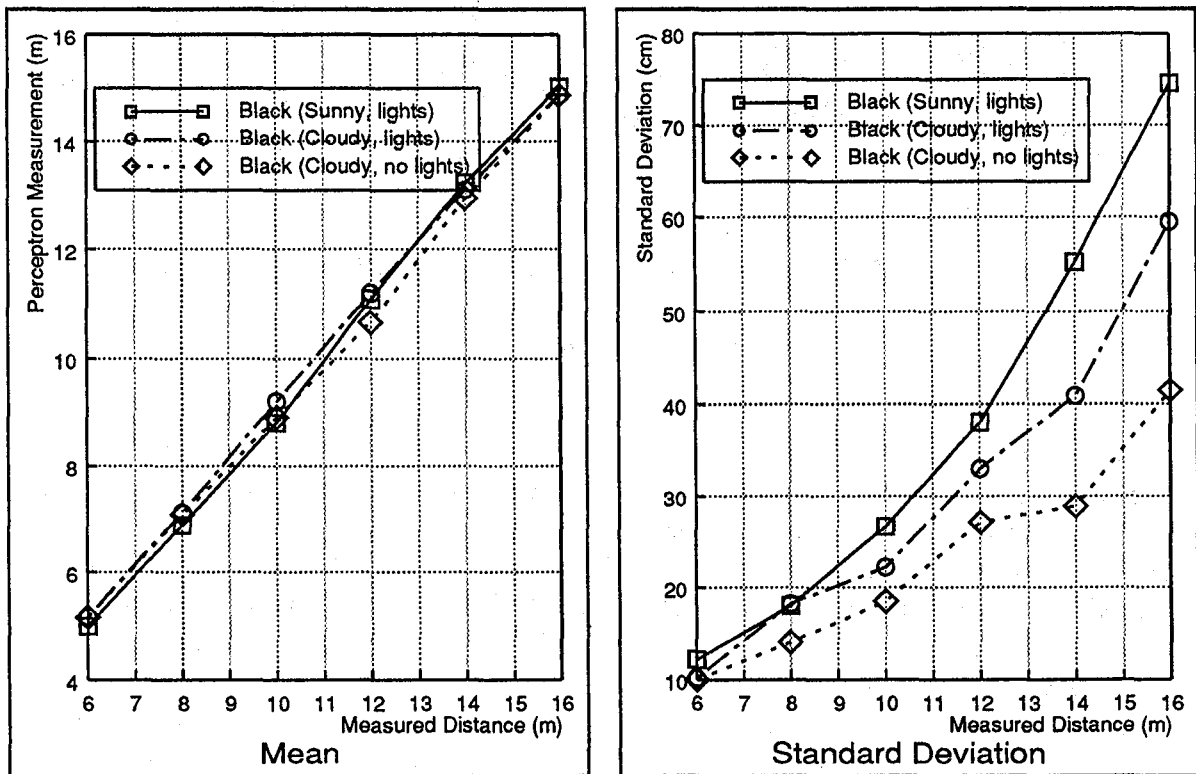


Figure 6.4: Range precision under different lighting conditions.

### Effect of Surface Material

Surface material has a definite effect on the range measurement. The highlighted region of the range image in Figure 6.5 consists of a flat, cement floor (gray color), with a dark grease spot.

Even though the distance should be constant, we observe different range values for the grease and the floor (shown in the magnified region to the right). We conclude that range measurements *do* depend on surface material, and we now quantify this.

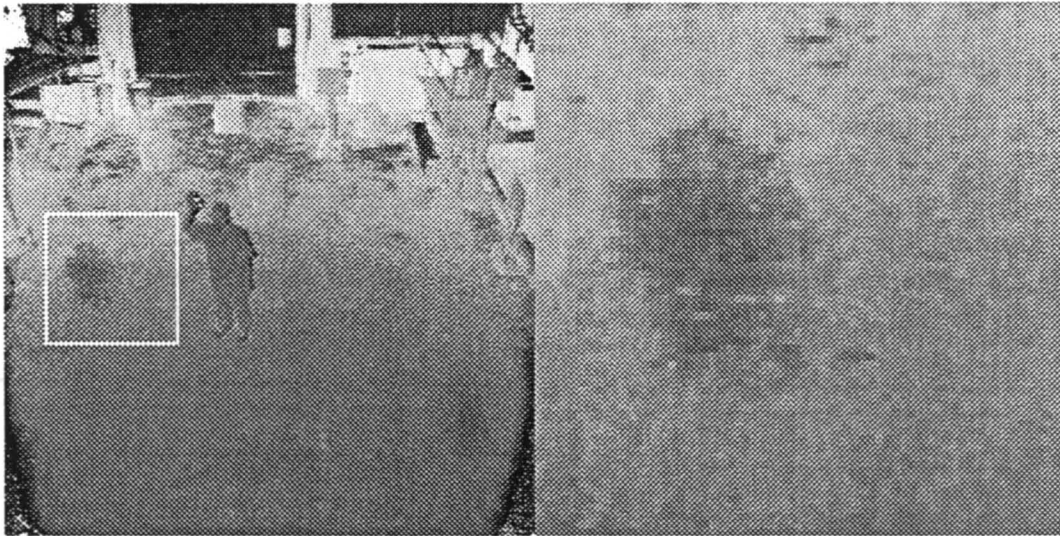


Figure 6.5: Range measurements differ across surface boundaries.

Range image on left, magnified region on right.

To investigate the effect of object surface material, we obtained range measurements from a variety of targets. Figure 6.6 shows the mean and standard deviation of range measurements for various targets at seven different distances. The left-hand side of the figure shows that the mean varies with different surface material. The right-hand side of the figure shows that when the returned reflectivity values from the target are large (the cardboard, gravel, and soil targets), the range measurements do not vary much, but when the reflected signal from the target is weak (the black target) we observe high variance.

This is a difference between the mean range values in Figure 6.6 and Figure 6.4 for the black target. We believe this is due to a change in the scanner's auto-zero circuitry. See appendix A for a discussion.

### Effect of Beam Incidence Angle

As the distance and incidence angle increase, the area of the footprint increases. As the area of the footprint increases, the precision of the range measurement significantly degrades. If we assume that the footprint is sufficiently small and  $\alpha$  is almost constant inside the footprint, the size of

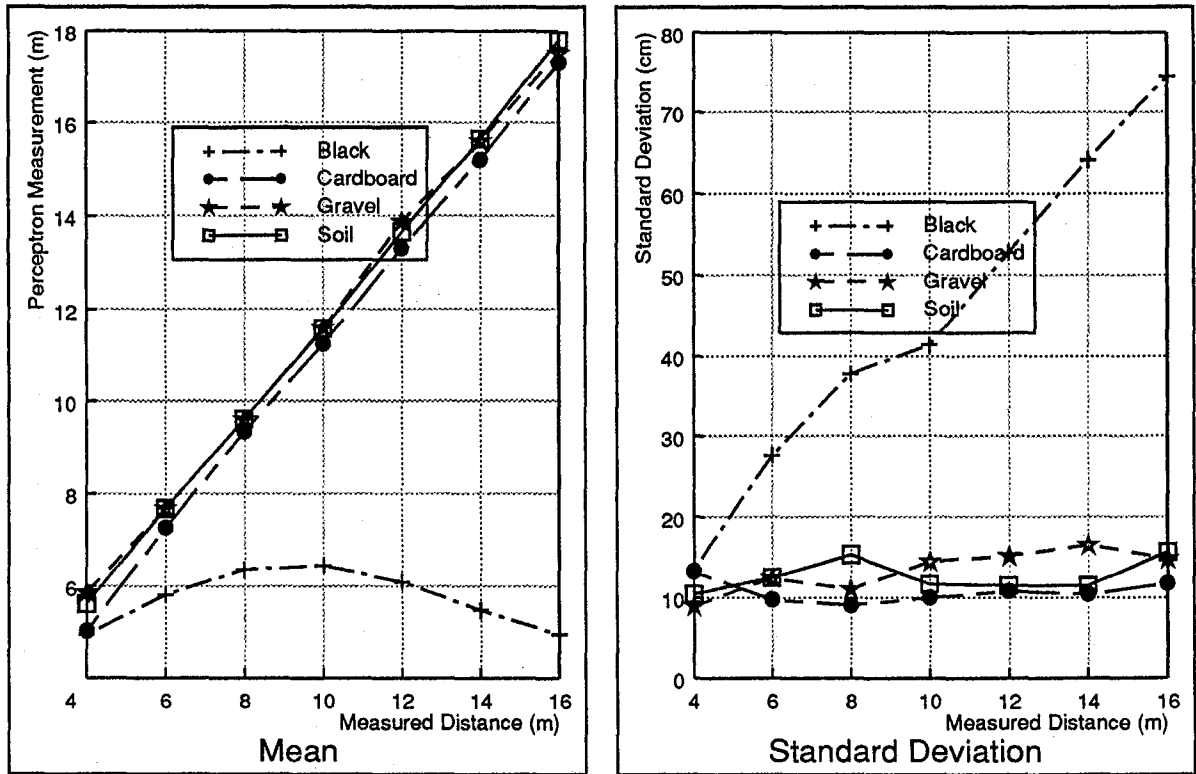


Figure 6.6: Range measurement statistics for different surface materials.

the footprint is roughly inversely proportional to  $\cos \alpha$ . A first-order approximation of the range precision  $\sigma_{range}$  is given by [5] as

$$\sigma_{range} \propto \frac{R_{\phi,\theta}^2}{\cos \alpha} \quad (6.2)$$

To verify this model, we conduct experiments in which we rotate the target to produce different incidence angles. To minimize the effect of ambient light on the range precision (see Section 6.2.2), we run these experiments at night.

Figure 6.7 shows the mean of the range measurements as a function of incidence angle and distance. We observe a variation in the mean of range measurements of about 10cm.

For incidence angle  $0^\circ$ , we fit a curve with  $\sigma_{range} = K_1 R_{\phi,\theta}^2 + K_2$ . For non-zero incidence angles, we fit the curves to Equation 6.2 by using the computed parameters  $K_1$  and  $K_2$  and the measured incidence angle  $\alpha$ .

Figure 6.8 shows the standard deviation of range measurements with different incidence angles. Circles indicate the measured  $\sigma$  from the experiment, and the curve is drawn from Equation 6.2. As predicted, we observe that the range precision degrades as the beam incidence angle becomes larger and as the distance increases. We also conclude that Equation 6.2 is a reasonable approximation for the Perceptron scanner for  $0^\circ \leq \alpha \leq 45^\circ$  and distance  $\leq 14\text{m}$ .

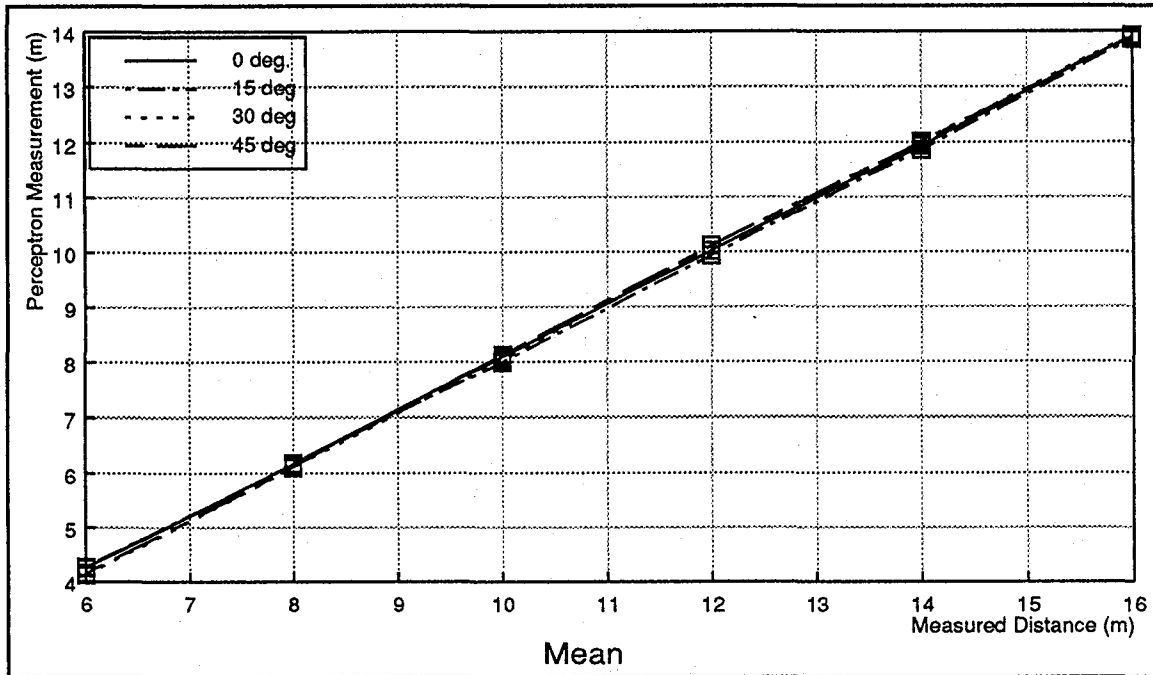


Figure 6.7: The mean of range measurements for different beam incidence angles.

### Effect of Temperature

Section 5.7 discussed qualitatively the problem of range drift. We believe long term drift is caused by changes in temperature, while short term fluctuations are due to noise in the sensor. Figure 6.9 shows the results of range measurements to a pair of targets over our normal ambient operating temperature of 65°F to 86°F. From 65°F to 75°F the mean values and standard deviation of the range measurement are roughly constant. Beyond this temperature range, the mean value of the range measurements increases with temperature. Surprisingly, the standard deviation of the range measurement peaks at about 81°F. We postulate that this is an effect of ambient sunlight. These measurements were taken during sunny, summer afternoons, from 12:00 to 6:00PM. The temperature of 81°F was reached about 3:00PM (when the ambient sunlight was at a maximum). The temperature inside the building increase for several hours, but the ambient sunlight diminished.

Our experience indicates that scanner remains calibrated between 65°F - 75°F. As the temperature increases, it is necessary to re-calibrate the scanner. In particular, temperatures above 80°F render the scanner unusable unless frequent re-calibration is performed.

Again we note some differences between temperature experiments possibly caused by a change in the scanner's auto-zero circuitry. See Appendix A for a discussion.

### Remarks

Possible causes of temporal variation of range measurements include the laser footprint and surface material. The laser footprint is the intersection of the laser beam, whose shape is a cone, with the target surface. Therefore, the size of the footprint increases with distance and with the angle  $\alpha$

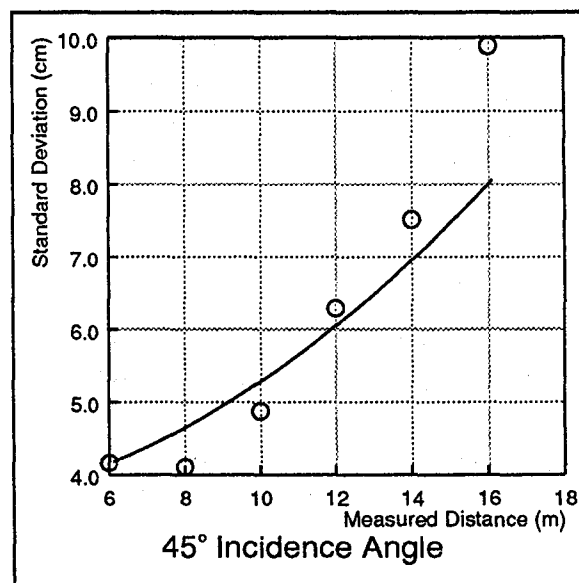
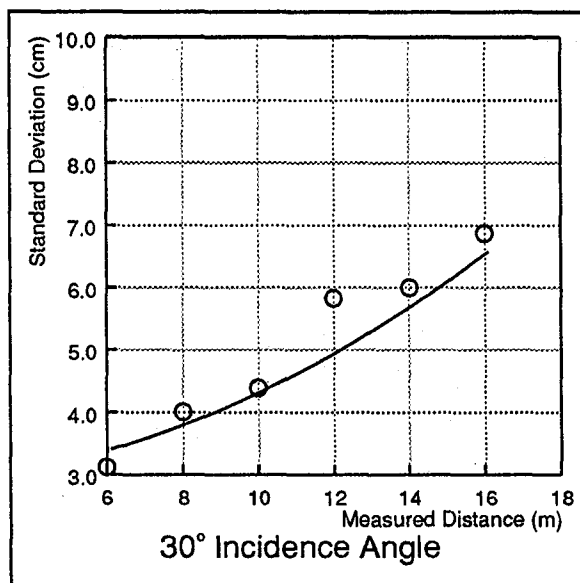
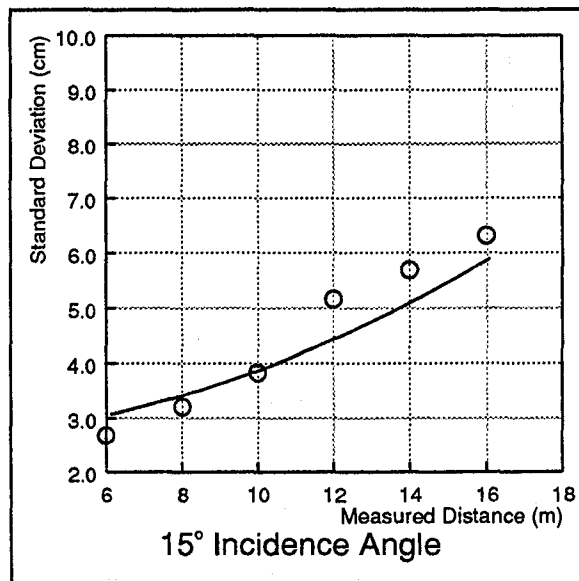
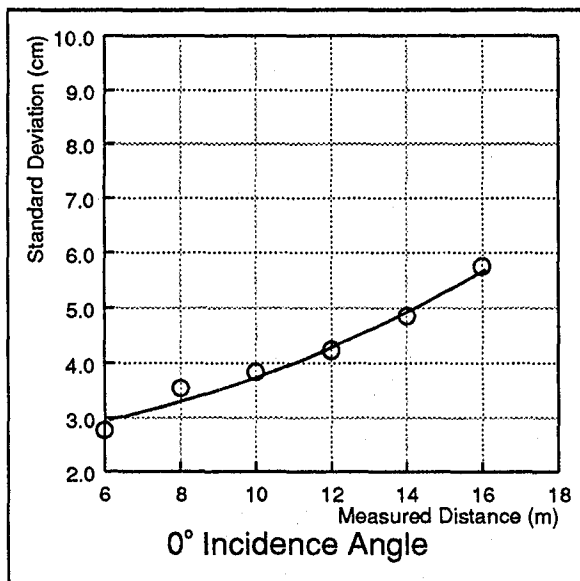


Figure 6.8: Standard deviation for different beam incidence angles.

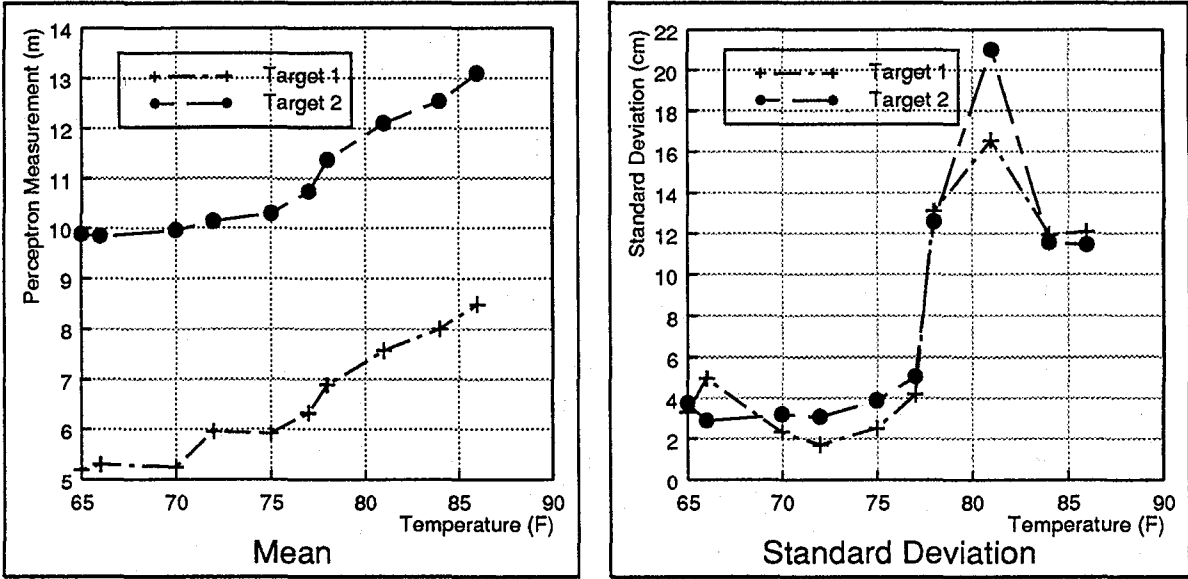


Figure 6.9: Range measurement statistics as temperature increases.

between the surface normal and the beam (the beam incidence angle). Since the measured range is a function of the range values over the footprint, the range precision depends on the distance and the beam incidence angle. The range precision may also depend on the amount of light reflected from the target, which again depends on the surface material and incidence angle.

### 6.3 Accuracy

To determine the accuracy of the range measurements is to identify the distance between them and the “true” ranges. For a target point lying in the direction  $(\phi, \theta)$ , let  $R_{\phi, \theta}$  be the range measurement reported by the scanner and let  $D_{\phi, \theta}$  be the true distance from the geometric origin as read from the tape measure (cf. Section 4.1). The sensor can only range objects that are at least 2m from the scanner, so  $D_{\phi, \theta} \geq 2$ . Under ideal conditions, we expect to observe a linear relationship:

$$R_{\phi, \theta} = aD_{\phi, \theta} + \rho_0 . \quad (6.3)$$

Here  $\rho_0$  is the distance from the origin to the (conceptual) surface corresponding to a range measurement of zero—we will call it the *offset distance*—and  $a$  is the slope. We expect that  $\rho_0 > 0$  because of the constraint on  $D_{\phi, \theta}$  and because the geometric origin is behind the scanner. We expect that  $a \approx 1$ , otherwise we do not know the ambiguity interval accurately.

We define  $\hat{D}_{\phi, \theta}$  as the estimate of the distance from the the scanner range measurement  $R_{\phi, \theta}$ .

This is given by:

$$\hat{D}_{\phi,\theta} = \frac{R_{\phi,\theta} - \rho_0}{a} \quad (6.4)$$

To determine the parameters  $a$  and  $\rho_0$ , we acquire range measurements of targets at known distances, and fit a line to the data. The slope and intercept are the parameters we seek. The detailed experimental procedure is as follows.

1. Adjust the stand so that the target is the same height as the scanner (80cm).
2. Tilt the scanner until the center of the target projects to row 127 in the reflectance image.
3. Position the target about 4m from the scanner, so that the target center projects to column 127 in the reflectance image, and the target is perpendicular to the vertical line. (Section 4.1 defines the vertical line.)
4. Move the target 2m away from the scanner, along the vertical line, so that the target still projects to column 127 and still is perpendicular to the vertical line.
5. Sense  $R_{\phi,\theta}$  100 times. Compute the mean and variance of the distribution of measurements.
6. Read  $D_{\phi,\theta}$  from the tape measure (cf. Section 4.1).
7. Repeat steps (4)–(6) a total of seven times. Thus, the final target position lies about 16m from the scanner.

We follow this procedure using different targets (one untreated cardboard slab, one cardboard slab painted black, one cover with gravel chips, and one covered with soil).

Figure 6.6 plots the results. It shows that the relationship between computed range and true range varies with target surface materials.

Table 6.1 shows the parameters extracted by fitting lines to data points in this graph. We observe the slope, intercept, and RMS error to vary with surface material. The RMS error gives some idea of the average accuracy of the scanner. Figure 6.10 plots the error  $D_{\phi,\theta} - \hat{D}_{\phi,\theta}$  as a function of true distance for various surface materials. It is difficult to discern any trends in the data. This is because the sensor noise ( $\sigma \approx 10 - 15\text{cm}$ ) dominates.

| Material  | $a$   | $\rho_0$ (standoff, m) | RMS Error (m) |
|-----------|-------|------------------------|---------------|
| Cardboard | 1.012 | 1.13                   | 0.08          |
| Gravel    | 0.983 | 1.85                   | 0.11          |
| Soil      | 1.01  | 1.56                   | 0.05          |
| Black     | -0.17 | 5.9                    | 0.56          |

Table 6.1: A line fit for computing the standoff distance.

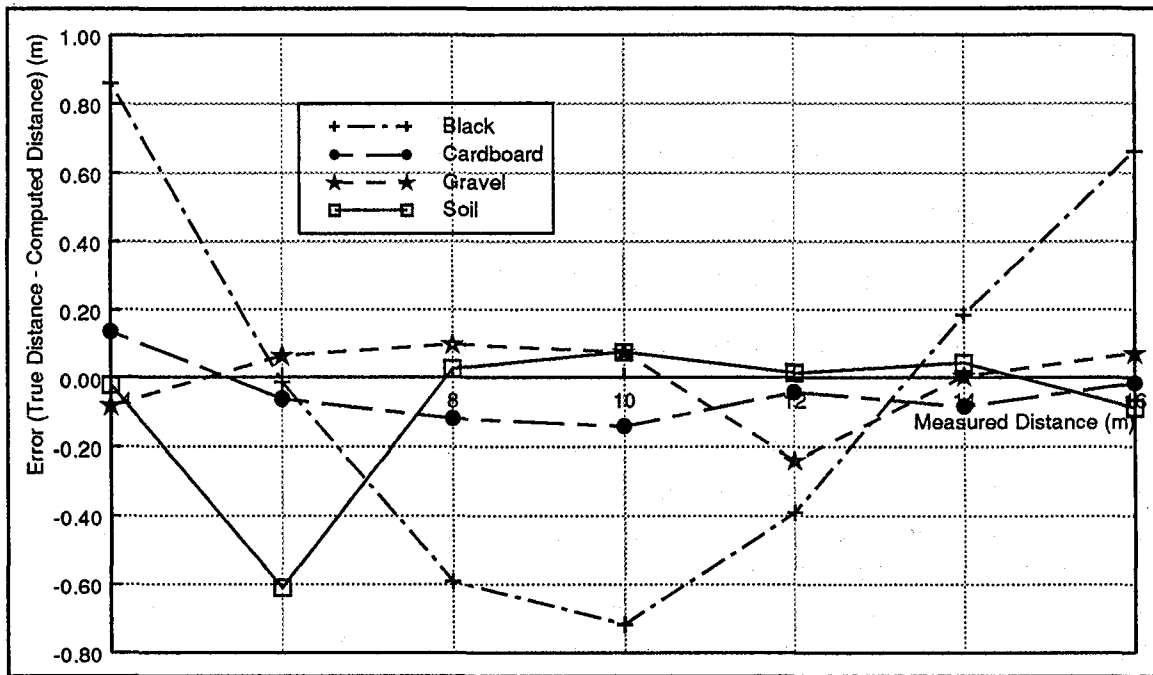


Figure 6.10: Sensor accuracy for different materials.

# Chapter 7

## Image Processing

This report has identified several problems with the Perceptron scanner. By understanding the types and sources of deficiencies in the scanner images, it is possible to minimize their effects. This section discusses the image processing techniques used to overcome these problems. The basic idea is to identify and mark pixels in the range image as being either valid (acceptable pixels), or conversely invalid (corrupted pixels).

### 7.1 Internal Reflections and Vignette Correction

Because these effects occur in constant, known positions, a simple range threshold operation can tag these pixels. The rectangles in the range image in the left-hand side of Figure 7.1 indicate the regions to which the thresholding operation is applied. The right-hand side of the figure shows the result of the threshold operation - white implies a valid pixel, black implies an invalid pixel.

Most of the vignette pixels and the smudge due to the internal reflection (lower right-hand corner) have been marked as invalid.

### 7.2 Surface Material Correction

Surface material problems occur when dark or black object appear in the scene. The manifestation of the problem is that dark objects may have range values 1 – 2m less than a correct value. We process the image to identify all unconnected regions in the image. We define connected not only in the sense of adjacent pixels in the image, but also connected in range (two pixels  $i.j$  and  $i+1.j$  are connected if  $|Range_{i.j} - Range_{i+1.j}| \leq \epsilon$ ). In the natural, outdoor cases we consider, all objects are smoothly connected to each other (i.e. there are no floating objects). Figure 7.2 shows the result of a connected region analysis. The range image on the left is processed to detect connected regions. The binary image on the right uses black values to indicate disconnected range pixels and white to indicate connected range pixels. Most of the pixels of the grease spot (see section 6.2.2 and Figure 6.5) have been marked as invalid. Also, other grease spot areas and a dark garage door at the top of the image have been tagged as invalid.



Figure 7.1: Range image and result of threshold operation.

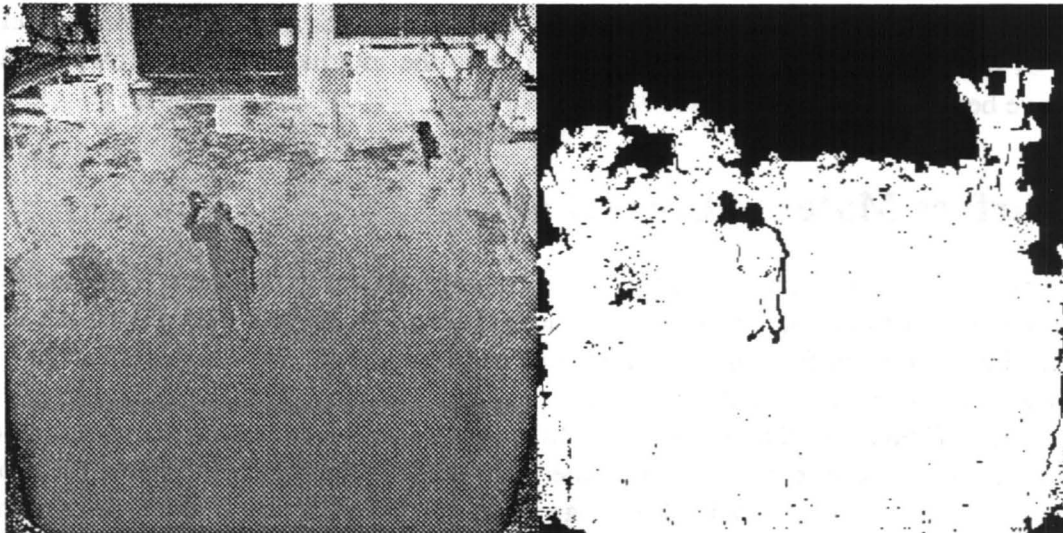


Figure 7.2: Range image and connected regions.

Combining the results of the thresholding and connected region analysis results in the image in Figure 7.3. In this image, 63% of the range image pixels have been identified as valid pixels. In our experience, this is a worst case - generally a much higher percentage of pixels are accepted.

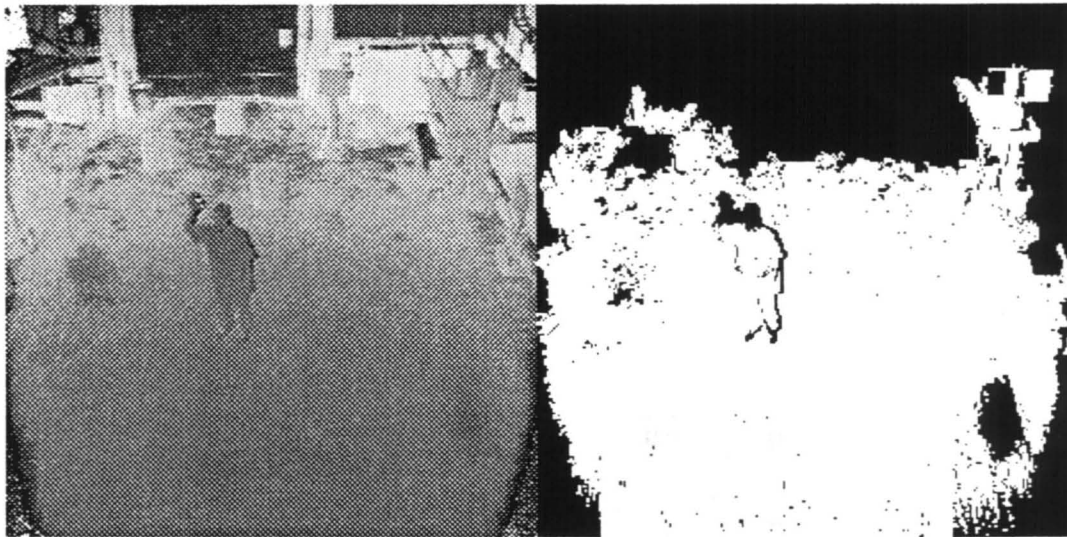


Figure 7.3: Range image and valid pixel mask.

### 7.3 Minimizing Statistical Variations

Statistical variations can be minimized by applying filters in both the spatial and temporal domains. Spatially, do adjacent pixels have similar range values, or is there significant noise? In the temporal domain, we are concerned with a sequence of images having a large standard deviation due to thermal noise and range drift. Of major concern are outliers - those pixels in the image that have significantly different values from their neighbors. A median filter is used to eliminate these outlying points. Table 7.1 summarizes statistics gathered for several planar targets in the image. In the spatial domain, we look at the statistics over a  $3 \times 3$ <sup>1</sup> pixel region - in the spatial domain, we take a sequence of seven<sup>2</sup> images and compute the standard deviation of the range measurement.

From this we note that spatially, there is little noise (on the order of 1-2 pixel counts). Temporally, the problem is more severe. We conclude that spatial median filter will do little to improve the image quality, but that temporal filter can increase the reliability of the range measurements.

---

<sup>1</sup>This size was chosen to reflect a typical  $3 \times 3$  median window size - anything larger tends to blur the image.

<sup>2</sup>This length yields acceptable run-time

| Target | Spatial $\sigma$ (cm) | Temporal $\sigma$ (cm) |
|--------|-----------------------|------------------------|
| 1      | 1.8                   | 7.9                    |
| 2      | 1.8                   | 6.8                    |
| 3      | 2.2                   | 8.0                    |
| 4      | 1.9                   | 5.4                    |
| 5      | 1.3                   | 5.4                    |
| 6      | 4.1                   | 7.1                    |
| 7      | 1.4                   | 7.9                    |

Table 7.1: Comparison of spatial versus temporal variations.

# Chapter 8

## Discussion

In this report, we have experimentally characterized the Perceptron laser rangefinder. We documented our experimental methods for evaluating and characterizing the scanner, and recorded many experimental results.

The experimental methods for determining the geometric parameters of the scanner—offset distance, field of view, and angular increments—are relatively straightforward and effective. Because the methods are simple, and because of further experience using the scanner with the computed geometric parameters to build quantitative maps, our confidence in the results is high. We believe that similar methods could be applied to similar sensors with virtually no modification, and equally good results. In the future, we hope to apply them to the Erim scanner.

The qualitative characterization of the sensor yielded results that are both surprising and disappointing. The existence of blatant flaws, such as internal reflections, vignette effects, skew in the upper portion of the field of view, range drift over time, and sensitivity to frame rate, raise disturbing questions about the implementation of the sensor. The existence of other problems, including the “shadows” appearing to the right of discontinuities, the sensitivity to ambient light and surface material, and the mixed pixel effect, arise due to inherent limitations of the rangefinding technology. In the future, we would like to extend the qualitative characterization of the sensor by more thoroughly decoupling and controlling the different causes and effects. As one example, we hope to study the effect of ambient light conditions on range measurements given targets at different distances and orientations, and with different surface materials. (For this, we might use the controlled imaging environment and high-precision equipment of the Calibrated Imaging Laboratory at CMU.)

The statistical characterization of the sensor was revealing, but perhaps not definitive. From the experimental results on precision, we conclude that pixel positioning is fairly precise, and that range measurement precision depends significantly on the intensity of ambient light, type of target surface material, target orientation with respect to the sensor, and temperature. From the experimental results on accuracy, we cannot draw unambiguous conclusions because of the difficulties in controlling variables such as temperature and incidence angle.

Qualitatively comparing the Perceptron scanner to the Erim scanner, the Perceptron furnishes more bits/pixel, larger images, and a higher data rate. We observe that the Perceptron senses

more meaningful range values from low-reflectance materials (i.e., it has a larger signal-to-noise ratio) and supplies more stable images with less jitter and distortion (i.e., it has a better scanning mechanism). In the future, we hope to compare quantitatively the two sensors in a comprehensive and systematic suite of experiments.

Interpreting the entire corpus of experimental results, we find that the performance of the Perceptron scanner does not compare favorably with the advertised performance, and that its nominal operating characteristics are not always observed in our experiments. We conclude that scanner repairs and modifications are required, and that further experimentation must be conducted. We are optimistic that these efforts will succeed, making the Perceptron scanner live up to its tremendous potential for three-dimensional active sensing.

# Appendix A

## Auto-zero Circuitry

Auto-zero circuitry within the scanner uses an internal target (at a known, fixed distance) to continually re-calibrate sensor readings. The auto-zero system compares the range measurement of the target to its known distance, and adds this error signal to the range image to correct for temporal drifting of the range values. During the course of the experiments, it was believed that this circuitry was functioning incorrectly, and the scanner was returned to the manufacturer for adjustment. This change had a deleterious effect on the scanner's sensitivity to surface materials. Compare the results for a black target from Figure 6.4 and Figure 6.6. The first data set was taken before the auto-zero change, the second set of data was taken after. The change increased the problem of incorrect range measurements of targets with low reflectivity.

To highlight this before and after difference, we show the results of an early experiment (before the auto-zero change) to test the effect of surface materials.

An experiment placed the black target on a larger cardboard target as shown in Figure A.1. To minimize any time drift effect, we capture 100 images and compute the mean and standard deviation of range measurements along a scan line with two different surface materials. We should not observe any depth difference between the two targets along the scan line.

The left figure in Figure A.2 shows range values along a row in the range image. The untreated cardboard target is visible between columns 115-120 and 136-140, and the black target is visible between columns 121-135. The range values for the cardboard and for the black target are essentially identical. This contrasts with the results from Figure 6.6 (taken after the auto-zero change) where the range measurements between the cardboard target and the black target vary significantly. After the change, the sensor range measurements became more sensitive to material properties. The right figure in Figure A.2 shows the standard deviation of range and reflectance measurements along the same row in the image. The range variations are larger for the black target than for the untreated cardboard target.

From this experiment, we concluded that the range means for the black and cardboard targets are identical. However, whenever we observe an abrupt change in reflectance across the boundary between the black and cardboard targets, we also observe an abrupt change in range (i.e., in the left figure, abrupt range changes exist at columns 122 and 135 where the boundaries of two surface materials exist). However, in reality, there is no depth discontinuity between the two different

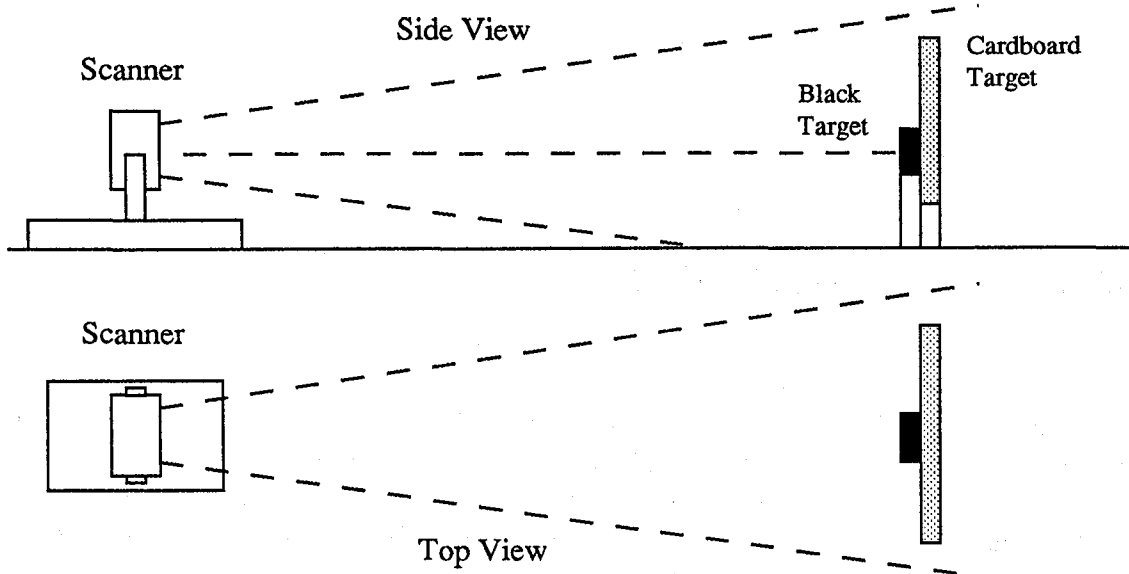


Figure A.1: Testing the effect of surface material on range measurements.

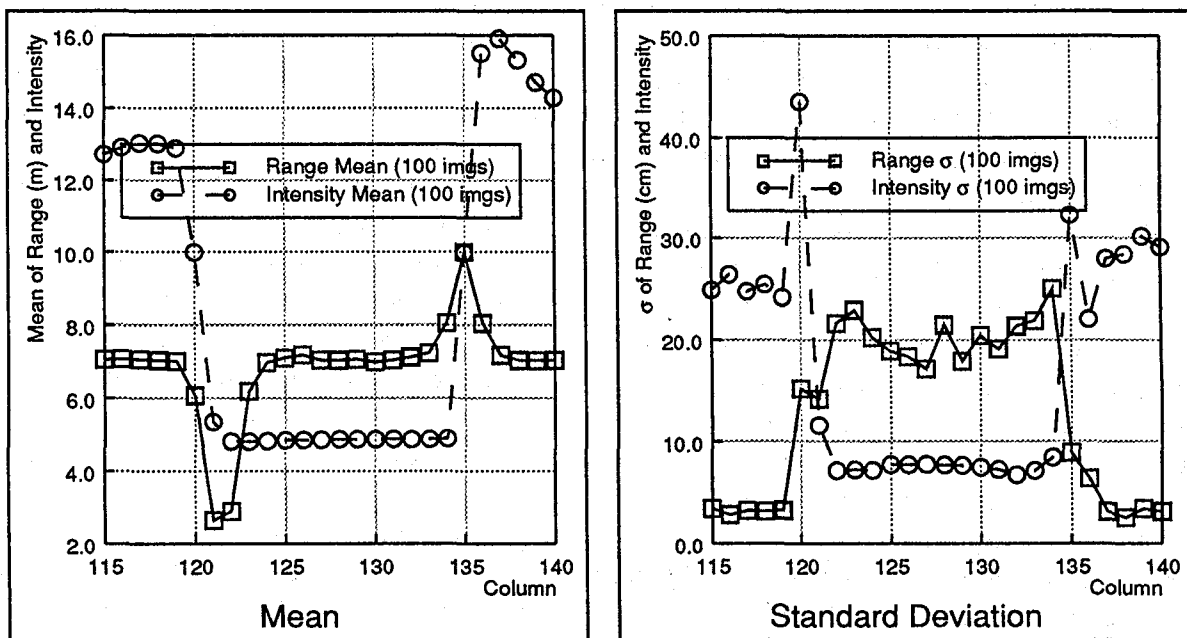


Figure A.2: Mean and standard deviation of range measurements across object boundaries.

surfaces. We speculate that the fluctuation in reflectance at the boundary could affect the phase difference measurement resulting in a range discrepancy.

A second change noticed was the effect of temperature on the range measurements. Compare the range drift results (Figure 5.10) with Figure 6.9. In the first case, the range measurement is inversely proportional to temperature, in latter case, the range is directly proportional to temperature.

## **Acknowledgements**

We would like to thank Takeo Kanade for his insights and helpful discussions throughout this work and Mike Blackwell for setting up the hardware and user interface. We would also like to thank Martial Hebert, Chuck Thorpe, and William Whittaker for their feedback. Thanks also to Brian Albrecht, Kevin Dowling, and Jim Martin for their help with the experimental setup.

# Bibliography

- [1] J. Bares, M. Hebert, T. Kanade, E. Krotkov, T. Mitchell, R. Simmons, and W. Whittaker. Ambler: An Autonomous Rover for Planetary Exploration. *IEEE Computer*, 22(6):18–26, June 1989.
- [2] P. Besl. Range Imaging Sensors. Technical Report GMR-6090, General Motors Research Lab, Warren, Michigan, March 1988.
- [3] P. J. Besl and R. C. Jain. Three-dimensional object recognition. *ACM Computing Surveys*, 17(1), March 1985.
- [4] H. Everett. Survey of Collision Avoidance and Ranging Sensors for Mobile Robots. *Robotics and Autonomous Systems*, 5:5–67, 1989.
- [5] M. Hebert and T. Kanade. 3-D Vision for Outdoor Navigation by an Autonomous Vehicle. In *Proc. Image Understanding Workshop*, Cambridge, Massachusetts, 1988.
- [6] M. Hebert, T. Kanade, E. Krotkov, and I. S. Kweon. Terrain Mapping for a Roving Planetary Explorer. In *Proc. IEEE Robotics and Automation Conf.*, pages 997–1002, Scottsdale, Arizona, May 1989.
- [7] R. Jain and A. Jain. *Analysis and Interpretation of Range Images*. Springer-Verlag, New York, 1990.
- [8] T. Kanade. *Three-Dimensional Machine Vision*. Kluwer Academic Publishers, 1987.
- [9] D. Nitzan. Assessment of Robotic Sensors. In *Proc. Intl. Conf. Robot Vision and Sensory Controls*, pages 1–11, London, England, April 1981.
- [10] Odetics, Inc., Anaheim, California. *3D Laser Imaging System*, 1989.
- [11] Perceptron, Inc., Farmington Hills, Michigan. *Laser Range Scanner for NavLab and Mars Rover Research*, May 1988. Perceptron Proposal 88038.
- [12] R. Simmons, E. Krotkov, and G. Roston. Integrated System for Single Leg Walking. Technical Report CMU-RI-TR-90-15, Robotics Institute, Carnegie Mellon University, Pittsburgh, Pennsylvania, July 1990.

- [13] P. Veatch and L. Davis. Efficient Algorithms for Obstacle Detection Using Range Data. *Computer Vision, Graphics, and Image Processing*, 50:50–74, 1990.
- [14] R. Watts, F. Pont, and D. Zuk. Characterization of the ERIM/ALV Sensor—Range and Reflectance. Technical Report , Environmental Research Institute of Michigan, Ann Arbor, Michigan, 1987.
- [15] D. Zuk, F. Pont, R. Franklin, and V. Larrowe. A System for Autonomous Land Navigation. Technical Report IR-85-540, Environmental Research Institute of Michigan, Ann Arbor, Michigan, 1985.



